AD_____

Award Number: W81XWH-10-1-0087

TITLE: Sympathetic Nerves in Breast Cancer: Angiogenesis and Antiangiogenic Therapy

PRINCIPAL INVESTIGATOR: Dr. Kelley S. Madden

CONTRACTING ORGANIZATION: University of Rochester
Rochester, NY 14611

REPORT DATE: February 2013

TYPE OF REPORT: Final

PREPARED FOR: U.S. Army Medical Research and Materiel Command
Fort Detrick, Maryland 21702-5012

REPORT DOCUMENTATION PAGE

Form Approved
OMB No. 0704-0188

1. REPORT DATE *(DD-MM-YYYY)*	2. REPORT TYPE	3. DATES COVERED *(From - To)*
February 2013	Final	1 February 2010 - 31 January 2013

4. TITLE AND SUBTITLE
Sympathetic Nerves in Breast Cancer: Angiogenesis and Antiangiogenic Therapy

5a. CONTRACT NUMBER

5b. GRANT NUMBER
W81XWH-10-1-0087

5c. PROGRAM ELEMENT NUMBER

6. AUTHOR(S)
Kelley S. Madden, Mercedes J. Szpunar, Edward B. Brown

E-Mail: kelley_madden@urmc.rochester.edu

5d. PROJECT NUMBER

5e. TASK NUMBER

5f. WORK UNIT NUMBER

7. PERFORMING ORGANIZATION NAME(S) AND ADDRESS(ES)
University of Rochester
Rochester, NY 14611

8. PERFORMING ORGANIZATION REPORT NUMBER

9. SPONSORING / MONITORING AGENCY NAME(S) AND ADDRESS(ES)
U.S. Army Medical Research and Materiel Command
Fort Detrick, Maryland 21702-5012

10. SPONSOR/MONITOR'S ACRONYM(S)

11. SPONSOR/MONITOR'S REPORT NUMBER(S)

12. DISTRIBUTION / AVAILABILITY STATEMENT
Approved for Public Release; Distribution Unlimited

13. SUPPLEMENTARY NOTES

14. ABSTRACT

Please see next page.

15. SUBJECT TERMS
breast cancer, sympathetic noradrenergic nerves, norepinephrine, adrenergic receptors, angiogenesis, multiphoton laser scanning microscopy

16. SECURITY CLASSIFICATION OF:			17. LIMITATION OF ABSTRACT	18. NUMBER OF PAGES	19a. NAME OF RESPONSIBLE PERSON
a. REPORT	b. ABSTRACT	c. THIS PAGE			USAMRMC
U	U	U	UU	74	19b. TELEPHONE NUMBER *(include area code)*

14. ABSTRACT

The sympathetic nervous system (SNS) is a major pathway activated by exposure to emotional stressors. We have demonstrated SNS 'hard-wiring' in the form of sympathetic nerve fibers in 4T1 mammary tumors, a mouse model of metastatic breast cancer. We established that 4T1 tumor cells do not express functional α- or ß-adrenergic receptors (AR), the receptors activated by norepinephrine (NE), the neurotransmitter of the SNS. Yet, manipulation of sympathetic neurotransmission *in vivo* by chemical ablation of sympathetic nerves to deplete NE decreased F480+ tumor associated macrophages and reduced tumor weight. Furthermore, chronic treatment with desipramine (DMI), an antidepressant that elevates synaptic NE, increased 4T1 tumor growth, but not metastasis. DMI-induced tumor growth was not associated with increased tumor angiogenesis, and pro-tumor cytokines VEGF, IL-6, RANTES, and MIP-2 were reduced by DMI. To further dissect the tumor response to NE, mice were treated with selective AR agonists. The α_2-AR agonist dexmedetomidine (DEX) increased tumor growth and metastasis in the absence of alterations in VEGF, IL-6, RANTES, and MIP-2. Treatment with the ß-AR agonists isoproterenol and salmeterol did not significantly alter tumor growth/metastasis. In DMI- and DEX-treated mice, tumor collagen microstructure was uniquely altered in 4T1 tumors, suggesting a novel stromal-mediated mechanism whereby elevated NE and stimulation of AR may increase tumor growth. These results suggest that NE-induced tumor growth is mediated by α_2-AR activation, but other AR pathways activated by elevated synaptic NE may modulate the tumor-promoting effect of α_2-AR activation. Understanding how AR pathways regulate breast tumor pathogenesis will lead to new therapies to inhibit tumor growth and metastasis.

Table of Contents

INTRODUCTION

Evidence from breast cancer patients and animal models of breast cancer suggests that stress can augment breast tumor growth and metastasis. Activation of the sympathetic nervous system (SNS) and release of norepinephrine (NE) from sympathetic nerve terminals is an important stress pathway. We have demonstrated such 'hard-wiring' in the mouse mammary fat pad in the form of sympathetic tyrosine hydroxylase (TH)+ nerve fibers that are associated with tumor blood vessels and within the tumor parenchyma in murine 4T1 mammary adenocarcinoma cells grown orthotopically in the mammary fat pad, but the functional interactions between sympathetic nerves and nearby target cells, including blood vessels, have not been investigated in breast cancer. We have demonstrated that catecholamine signaling can induce VEGF expression in some breast tumor cell lines *in vitro* (1). Consequently, we believe that *SNS innervation is a key factor in encouraging angiogenesis, in preserving innervated tumor vessels from antiangiogenic therapy, and in providing a framework for rapid revascularization after effective therapy ceases.* We further believe that *therapeutic targeting of SNS signaling, using reagents already available in the clinic, is a promising method for inhibition of angiogenesis that will be synergistic with current antiangiogenic therapies and will greatly attenuate revascularization after effective therapy ceases.* Therefore, we propose to examine the impact of sympathetic innervation on angiogenesis and antiangiogenesis. We will test the following hypothesis: **Sympathetic innervation of breast tumors promotes angiogenesis and protects tumor blood vessels from antiangiogenic therapy.** Our first objective is to delineate the role of breast tumor sympathetic innervation and NE signaling in tumor growth, angiogenesis, and metastasis. A second objective is to explore the dynamic effect of catecholamine signaling on tumor vasculature using *in vivo* imaging with multiphoton laser scanning microcopy (MPLSM). The specific aims to achieve these objectives, broken down into individual tasks and progress made for each individual task, are described below. The time frame provided in parentheses after each task was taken from the statement of work.

BODY

Specific Aim 1. Determine how manipulation of sympathetic input influences breast cancer growth, angiogenesis, and metastasis.

Task 1. Initiate experiments to assess impact of sympathetic neurotransmitter removal/blockade in 4T1 tumors.

Methods.

Experimental Procedures.

Orthotopic Tumor Implantation and Measurement. 4T1 tumor cells were grown as described in the attached manuscript. 4T1 cells ($1x10^5$ in sterile saline) were injected into the third mammary fat pad (MFP) under ketamine/xylazine anesthesia. Tumors were measured with calipers every 2-3 days without knowledge of experimental group. Mice were sacrificed by pentobarbital overdose (200 mg/kg, IP) followed by cervical dislocation to harvest tumor, spleen, and lungs. Tumors and spleens were weighed and divided. For catecholamine and cytokine analyses, tissue was immediately placed on dry ice and stored at -80°C.

Tumor volume (V) was calculated using the equation $V=1/2*length*width^2$. Tumor growth is presented as normalized tumor growth. Normalized tumor growth was calculated by dividing an individual's tumor volume at a given time point by its volume at the earliest time point all tumors were detected (between days 3 and 5 post-4T1).

For sympathetic ablation, 6-OHDA was administered intraperitoneally (IP) 4 and 2 days prior to tumor implantation and thereafter every 5 days to prevent reinnervation and maintain a long-term

sympathectomy (2). The vehicle for 6-OHDA (0.01% ascorbate dissolved in saline) was injected IP into control animals in parallel with 6-OHDA treatment.

For DMI treatment, mice were implanted subcutaneously with 21-day slow release implantable pellets (Innovative Research of America, Sarasota, FL) containing desipramine or placebo pellets. Alternatively, DMI was injected IP daily and continued for the duration of the experiment. DMI was prepared for injection by solubilizing in a small volume of sterile endotoxin-free water and diluting to the final concentration with sterile saline. The vehicle was prepared exactly the same way without the DMI.

To block ß-AR, mice were implanted subcutaneously with 21-day slow release implantable pellets (Innovative Research of America) containing either 0.5 or 5 mg nadolol or placebo.

For preparation and treatment with ISO, DEX, and PE, see attached manuscript.

Immunocytochemistry and second harmonic generation (SHG). Tumors were processed for immunocytochemistry and SHG as described in the attached manuscript. Details of imaging and image analysis procedures are described in the attached manuscript. Images were analyzed using Image J.

Determination of NE, NMN, and cytokines/chemokines.

Tumors were homogenized and lysates prepared as described in the attached manuscript. ELISAs and multi-analyte analysis using a Milliplex mouse cytokine/chemokine magnetic bead panel kit (Millipore, catalogue #MCYTOMAD-70K) were employed as described in the attached manuscript. In two experimental repetitions, NE and NMN concentration differed and therefore the data are normalized, based on percent of placebo control response at each time point. For each experimental repetition, the average NE or NMN in placebo-treated mice at each time point was calculated. The NE and NMN concentration in each individual placebo- and DMI-treated mouse at that time point was divided by the average placebo response. Thus the normalized results presented in Fig. 2 represent the percent of the average placebo control response at that time point.

Metastasis. Lungs were prepared and processed as described in the attached manuscript.

Flow Cytometry. Spleen or tumor single cell suspensions were prepared by pressing tissue through a metal mesh into ice-cold PBS containing 10% fetal calf serum (PBS-FCS). Red blood cells were lysed using ammonium lysis buffer. After washing twice in PBS-FCS, the cells were counted and resuspended to $1.5x10^6$ cells per ml in phosphate buffered saline containing 1% bovine serum albumin and 0.25 % sodium azide (flow wash). Cells were centrifuged, and macrophages, neutrophils, and myeloid derived suppressor cells were detected using three-color immunofluorescence. Cells (1.5×10^6) were incubated in 25 µl FcBlock (anti-CD16, diluted 1:50; BD Biosciences, bdbiosciences.com) for 15 minutes at 4˚C. Rat anti-F4/80 (clone BM8; FITC-conjugated; Abcam Inc.; abcam.com), rat anti-CD11b (clone M1/70; Alexafluor 647-conjugated, BD Biosciences) and rat anti-Gr-1 (anti-Ly-6G and Ly-6C; clone RB6-8C5; PE-conjugated; BD Biosciences) were diluted 1:50 in flow wash. Antibodies (100 µl) were incubated 30 min at 4 °C. Cells incubated in flow wash only served as autofluorescent controls. For color compensation, cells were incubated with each of the three antibodies separately. After incubation with the antibodies, cells were washed two times in flow wash, fixed in 0.5 ml PBS containing 1% paraformaldehyde, and stored in the dark at 4 °C for no longer than 2 weeks before analysis. Fluorescence was analyzed in the University of Rochester Flow Cytometry Core on a BD LSR II 18-Color flow cytometer. Initial gating was based on forward scatter versus side scatter bitmap gating. Analysis gates were set based on autofluorescent controls.

Statistical Analysis. In experiments in which two groups were compared, an unpaired two-tailed student's t-test was conducted. If the F-test for variance was significant, indicating that variability differed between the two groups, then a non-parametric Mann-Whitney U-test was used instead. To compare more than two groups, ANOVA was used. For one-way ANOVA, significant main effects were analyzed by

Newman-Keuls post-hoc analysis. For two-way ANOVA, significant main effects or interactions between the two variables were analyzed by Bonferroni's post-hoc or Holm-Sidak multiple comparison tests. Tumor growth over time was analyzed using a repeated measure ANOVA, and significant interactions between treatment and time were analyzed using Holm-Sidak multiple comparison tests. In all statistical analyses, $p<0.05$ is considered statistically significant.

Results.

Specific Aim 1. Determine how manipulation of sympathetic input influences breast cancer growth, angiogenesis, and metastasis.

Task 1. Initiate experiments to assess impact of sympathetic neurotransmitter removal/blockade in 4T1 tumors.

We used 6-hydroxydopamine (6-OHDA) as a means to ablate the sympathetic nervous system in the periphery of adult mice. In the previous two annual reports we showed that 6-OHDA treatment markedly reduced NE in spleen and 4T1 tumors. Ablation of sympathetic neurotransmission throughout tumor growth decreased tumor and spleen weights with no change in tumor metastasis. The reduction in tumor weight was associated with reduced F4/80+ tumor macrophages and decreased tumor production of IL-6 in sympathectomized mice.

We also tested the effect of chronic treatment with the non-selective ß-AR blocker nadolol. The results shown in Fig. 1 are representative of experiments testing implantation of 0.5 mg or 5 mg nadolol 21-day release pellets two days prior to 4T1 injection. These groups were part of experiments designed to identify the AR driving DMI-induced tumor growth (DMI results are discussed below). Unfortunately, the combination of DMI and nadolol treatment produced an unacceptably high mortality rate, suggesting that ß-AR activation countered toxic effects of DMI treatment. We show here the results of the groups from these experiments that received nadolol and placebo pellets. We should note that implantation of placebo pellets or pellets containing 0.5 or 5 mg nadolol resulted in no deaths. Fig. 1 demonstrates that chronic nadolol treatment does not significantly alter tumor progression. Nadolol treatment had no impact on tumor growth, VEGF, or IL-6 production compared to placebo controls.

Discussion/Conclusions. The reduced tumor weight in sympathectomized mice indicates that the intact sympathetic nervous system can drive tumor growth. Furthermore, the sympathectomy-induced reduction in tumor NE suggests that the sympathetic nerves innervating 4T1 tumors may be a mechanism underlying SNS regulation of tumor pathogenesis. However, because sympathetic nerves are ablated throughout the periphery, it is possible that loss of sympathetic nerves in other organs may contribute to 4T1 pathogenesis and the 6-OHDA-induced reduction in tumor weight. Specifically, the reduced spleen weight and decreased tumor macrophages in sympathectomized animals suggests that the loss of sympathetic input may result in reduced production of the hematopoietic cells that populate the spleen and tumor in mice bearing 4T1 tumors (3). Therefore SNS activation can increase tumor associated macrophages to promote tumor growth. Sympathetic innervation of spleen and/or bone marrow or the tumors themselves may drive differentiation and/or tumor infiltration of tumor associated macrophages.

The negative results with ß-blockade indicate that under our experimental conditions, ß-AR do not play a significant role in modulating tumor pathogenesis. On the other hand, the unexpected deaths associated with combined DMI (to elevate synaptic NE) and nadolol (both 0.5 and 5 mg pellets) suggest that nadolol was effective at blocking ß-AR. In this experiment, after the pellet implantation and 4T1 injection, mice were exposed to regular handling required to measure tumor volume. These results imply that relatively mild daily stressors were not sufficient to alter tumor pathogenesis via NE release and ß-AR activation, and is consistent with the relatively low affinity of NE for ß-ARs.

Task 2. Initiate experiments to assess impact of elevation of NE in 4T1 tumors

Since the last annual report, we have continued experiments using the tricyclic antidepressant, desipramine (DMI) to block NE uptake and thereby increase synaptic NE. In the previous reports, we described the impact of chronic DMI treatment using implanted continuous release pellets containing various doses of DMI. In addition, we initiated experiments to define the AR(s) involved in NE regulation of tumor pathogenesis. Most of the results from these experiments were included in the last annual report, and are presented in the attached manuscript that has been submitted for publication. In this report, the results of the experiments that have been conducted since the last DOD annual report will be discussed in the context of the previous findings.

DMI Dose Response: High dose DMI increased tumor growth without altering metastasis to the lungs. In the last report, we showed that 5 mg and 7.5 mg DMI continuous release pellets, implanted 2 days prior to 4T1 injection, did not alter tumor growth or metastasis relative to animals that received placebo pellets, despite evidence for elevated NE and NMN in tumors and in spleen. The 7.5 mg dose also significantly decreased tumor VEGF and slightly decreased tumor IL-6. At 10 mg, DMI significantly increased tumor growth and tumor weight (Fig 2A-C; attached manuscript). These changes were not associated with detectable changes in CD31+ blood vessel density (Supplemental Fig. S3, attached manuscript). Multiplex analyte analysis revealed that TNF-α was elevated with DMI treatment, and several chemokines that are associated with tumor progression were significantly decreased (RANTES and MIP-2) or trending towards reduced production, including MCP-1 and M-CSF (Fig. 4A, attached manuscript) (4). DMI treatment did not alter the proinflammatory cytokine IL-1ß, the T cell-associated cytokines IL-2 and IFN-γ or the anti-inflammatory cytokine IL-10 (see previous annual report). To determine if elevated TNF-α could induce tumor cell proliferation, we added TNF-α to 4T1 cells in vitro and measured proliferation using the Cy-Quant proliferation assay. Varying concentrations of TNF-α did not alter 4T1 proliferation (Supplemental Fig. S4; attached manuscript), suggesting that other mechanisms underlie the DMI-induced increase in tumor growth.

The chemokines RANTES, MIP-1, MCP-1, and M-CSF facilitate tumor infiltration by macrophages and/or neutrophils (4, 5). Therefore, we predicted that these populations may be reduced in DMI-treated mice. When the 10 mg DMI time course experiment was repeated, flow cytometry was included to analyze different tumor infiltrating populations in tumors and in spleen. In the spleen, the frequency of F4/80+ macrophages was transiently increased day 7 post-4T1 inoculation, but was not altered at either time point examined in the tumors (Fig. 2A,B). The percentage of Gr-1+ neutrophils was not altered in the spleen or the tumors (Fig. 2C,D). (In Fig. 2C, note the dramatic increase in neutrophils in the spleen over time, as reported by (3)). The percentage of myeloid derived suppressor cells (CD11b+Gr-1+) cells in spleen and tumor were not changed day 7 after 4T1 inoculation (Fig. 2E,F). (Unfortunately, at day 12 CD11b staining was not done). These results do not provide any indication of significant reductions in the percentages of macrophage/monocyte or neutrophil populations in tumors from DMI-treated mice. However, a functional analysis of these populations may reveal alterations with DMI treatment.

In the previous report, we introduced the idea that measuring NE alone may underestimate the amount of extracellular NE available for stimulation of AR, because increased synaptic NE may be compensated for by several mechanisms, including decreased TH synthesis or an accelerated rate of NE uptake into sympathetic nerve terminals (6). To confirm that NE in the synapse is increased with DMI treatment, we measured the NE metabolite normetanephrine (NMN). The production of NMN from NE is catalyzed by catechol-o-methyl transferase (COMT), an enzyme found only outside nerve terminals (6). We showed that splenic NE and NMN were markedly elevated 3 days after DMI implantation relative to placebo controls, with a greater increase in NMN compared to NE in DMI-treated mice (Supplemental Fig. S2A,B; attached manuscript), confirming that DMI elicited a transient elevation in synaptic NE in the periphery of mice implanted with 10 mg DMI pellets. In the previous annual report, tumor NE and NMN

were not elevated by chronic DMI treatment at least at the later time points examined. In the current report, results are presented that examine earlier time points in tumor development.

DMI transiently elevates synaptic NE in the periphery. A time course following 10 mg DMI pellet implantation was repeated with an additional measurement of NE and NMN earlier in the development of the tumor. NE and NMN concentrations from the two experimental repetitions were normalized for presentation in Fig. 2. Tumor NE and NMN were not significantly altered at any time point, although a trend toward increased tumor NMN at day 12 post-4T1 inoculation was noted (Fig. 2A, B). Splenic NE concentration was increased only at day 14 post-4T1 injection, but splenic NMN was elevated at d 7 and d 14 post-4T1 in DMI-treated mice. DMI elevated splenic NMN approximately 2-fold at day 14, a magnitude that is greater than the increase observed in NE (approximately 1.5-fold increase) (Fig. 2C,D). (See figure legend for statistical analyses).

Daily DMI Injections. With the continuous release formulation used here, DMI is released into the bloodstream at a constant rate thus maintaining a constant plasma concentration of DMI. We wondered if, under these conditions, the impact of NE uptake inhibition on synaptic NE was more readily attenuated by homeostatic mechanisms, limiting the impact of NE uptake inhibition. We hypothesized that daily bolus injections (IP) of DMI with peaks and valleys in plasma DMI concentration, would limit the homeostatic response and thereby induce a greater elevation in NE/NMN and a correspondingly greater increase in tumor growth. To test this possibility, mice were injected with DMI (5 mg/kg) daily beginning two days prior to 4T1 injection and continuing until animals were sacrificed at day 14 post-4T1 inoculation. The dose of DMI was chosen based on the DMI dose that can block 6-OHDA-induced sympathectomy in mice (7). To ablate sympathetic nerves, 6-OHDA must be taken up through the same NE uptake mechanism that is blocked by DMI. Daily DMI injection increased the rate of tumor growth similar to that induced by the continuous release of DMI (Fig. 4A), but tumor VEGF and IL-6 were not altered at the time of sacrifice (Fig. 5A,B). Tumor TNF-α was not detectable in tumors from this experiment. Daily DMI treatment did not significantly alter tumor NE at either day 9 or at day 16 post-4T1 treatment, but tumor NMN was significantly elevated at day 9 post-4T1 injection (a time point just prior to DMI-induced tumor growth) (Fig. 4B,D). Neither spleen NE or NMN were elevated at either time point in DMI treated mice (Fig. 4C,E), suggesting that the late elevation in spleen NE and NMN with subcutaneous continuous release DMI requires continuous NE uptake inhibition.

Discussion/Conclusions. Daily DMI treatment did not induce greater tumor growth than continuous DMI treatment, as we had predicted. Daily DMI treatment did not significantly elevate spleen NE or NMN at the time points examined. However, in the tumor, NMN was transiently elevated at a time just prior to increased tumor growth. This DMI-induced increased in tumor NMN suggests that DMI can enter the tumor tissue and transiently elevate synaptic NE (as measured by tumor NMN), and is consistent with the ability of 6-OHDA to enter tumors to destroy sympathetic nerves and deplete tumor NE, as shown in the previous DOD annual report. These results confirm that we can reliably measure changes in tumor NE and NMN even at late time points in tumor growth when tumor NE and NMN concentration is quite low.

Another important finding that is apparent from this time course study and the results in the previous report: there is a clear relationship between increased tissue volume (in the spleen and tumor) and decreased NE and NMN concentration (e.g. see Figure 4 and previous annual report). This negative relationship between tissue volume and NE concentration suggests that activation of the sympathetic nervous system will have a decreasing influence in these tissues as the tumor grows. With regards to the late DMI-induced elevation of NE and NMN in the spleen, the timing of this increase, corresponding to a large, and fairly rapid increase in tissue volume, leads us to speculate that any homeostatic mechanisms that are induced by constant exposure to DMI and increased synaptic NE are removed once NE concentration drops below a certain threshold with rapid expansion of spleen volume. NE reuptake inhibition by DMI appears to help compensate for the reduced NE concentration. It is not clear why a

similar mechanism is not active in the expanding tumors (for example, at day 14-16 post-4T1 injection). It is possible that the ability of DMI to elevate NMN in the tumor may be transient with the rapid increase in tumor volume in the DMI-treated mice and therefore it may be difficult to pin-point the exact time. Alternatively such a compensatory mechanism in response to decreasing NE concentration may be apparent only in more highly innervated tissues.

Overall, our results provide evidence for dynamic changes in synaptic NE concentration in spleen and tumor with continuous and daily DMI treatment, but the inability to show significant changes in NE/NMN in the tumor in the context of DMI-induced tumor growth suggests that elevated NE in other non-tumor sites may be primarily responsible for the elevated tumor growth. An important question that arises from these studies is what AR can drive tumor growth. The DMI experiments demonstrate that elevated synaptic NE can stimulate tumor growth, but NE can activate both α-AR and ß-AR. Here we summarize our previous results treating mice with selective AR agonists and measuring tumor growth and metastasis and present results of further analyses of these *in vivo* AR agonist experiments.

AR Agonist Experiments. In the previous annual report, we presented results using treatment with AR agonists to selectively activate AR *in vivo*. The AR agonists ISO, a non-selective ß-AR agonist, phenylephrine (PE), an α_1-AR agonist, and dexmedetomidine (DEX), a highly selective α_2-AR agonist were injected IP, once per day, beginning two days prior to 4T1 inoculation and continuing until sacrifice. This experimental treatment mimicked that of other investigators who reported increased tumor pathogenesis following ß-AR stimulation with ISO (8). We found that tumor growth, tumor weight at sacrifice, and metastasis were not significantly altered by ISO or PE treatment (Figs. 3A-D; attached manuscript). On the other hand, both doses of the α_2-agonist DEX increased tumor growth and metastasis (Figs. 3G-J; attached manuscript). Neither tumor VEGF or IL-6 were altered by ISO or DEX (Figs. 3E,F,K,L; attached manuscript). Based on the multi-analyte analysis, DEX treatment did not significantly alter other tumor cytokines or chemokines except for a trend in increased TNF-α production (Fig. 4B; attached manuscript).

Since the last annual report, we have completed the multi-analyte analysis of tumor homogenates from the PE and ISO experiments (Fig. 6). No significant changes were detected in any of the 14 chemokines and cytokines tested, with the exception of decreased production of the T cell cytokine IL-2 with PE treatment (and a trend noted with IL-2 with ISO treatment). Of the chemokines that were reduced in DMI-treated mice, trends toward reduced production were noted with MCP-1 (PE) and RANTES (ISO).

We noted a trend towards reduced growth with chronic daily ISO treatment (Figs. 3A; attached manuscript day x treatment interaction, $p = 0.14$). To further investigate potential ß-AR-induced effects on tumor growth, we tested chronic salmeterol treatment *in vivo*. Salmeterol is a so-called 'long-lasting' $ß_2$-AR agonist used in the treatment of asthma. It has high affinity for $ß_2$-AR, but is unable to desensitize ß-AR, resulting in a long-term effectiveness that cannot be achieved with most ß-agonists (9). This experiment has just been completed, and we have a few results to report here. Mice were treated with 5 mg/kg salmeterol or saline beginning 2 days prior to 4T1 injection. Once daily injections continued until the day of sacrifice, day 19 post-4T1 inoculation. Tumor growth was not significantly in salmeterol-treated mice (although a slight reduction similar in magnitude to that of ISO treatment was noted) (Fig. 7A). Tumor VEGF was slightly, but significantly, increased in salmeterol-treated mice (Fig. 7B), but IL-6 was not altered at this time point (Fig. 7C). By flow cytometry, the frequency of the tumor myeloid derived suppressor cell population (CD11b+Gr-1+) was significantly reduced in salmeterol-treated mice, but no alterations were detected in the CD11b+ Gr-1- (monocyte) or CD11b-Gr-1+ (neutrophil) populations (Fig. 8D). Representative single and two color histograms for distinguishing the CD11b/Gr-1 populations are shown in Fig. 8A-C. We are currently awaiting the results from multi-analyte analysis and quantification of lung metastasis in salmeterol-treated mice.

Conclusions/Discussion. We treated mice with adrenergic agonists selective for α-AR or ß-AR. Neither PE, an α_1-AR agonist, nor the ß-agonists ISO or salmeterol recapitulated DMI effects on tumor growth. Instead, our results demonstrated that DEX-induced α_2-AR activation can drive tumor growth and metastasis. The ß-agonist results suggest trends toward reduced tumor growth, consistent with reduced tumor myeloid derived suppressor cell populations (10), but thus far, we lack statistically significant evidence that ß-AR stimulation inhibits 4T1 tumor growth. ß-AR activation may elicit more subtle effects that require more careful examination of such variables as timing of drug administration relative to tumor initiation and duration of treatment. Treatment duration may be more relevant to ß-AR agonists that down-regulate ß-AR (such as ISO), but the salmeterol experimental results suggest that the inability to elicit a more dramatic impact on tumor growth is not due to receptor down-regulation.

The ability of DMI, but not DEX, to reduce pro-tumor chemokines (DMI) and ß-AR stimulation (salmeterol) to reduce pro-tumor MDSCs suggests that ß-AR stimulation may have the capacity to counter-act the pro-tumor effects of α_2-AR activation. This is an interesting hypothesis that needs to be further explored especially in the context of stress-induced sympathetic activation and NE release. Despite the uncertainty as to the pro-tumor mechanism of action of these drugs, the findings are particularly relevant because of the use of DMI and DEX in clinical populations, including breast cancer patients (11-14).

4T1 as a model of AR-negative breast cancer

One reason we are particularly interested in ß-AR-induced effects on tumor pathogenesis is because several reports demonstrated a role for ß-AR in stress-induced tumor pathogenesis, including increased tumor growth and metastasis (8, 15). These effects were mediated at least in part through increased tumor angiogenesis. However, we find no evidence for alterations in blood vessel density with DMI treatment (Supplemental Fig. S3; attached manuscript). An important difference between the tumor cell lines used in these reports and the 4T1 tumor model used here is the expression of ß-ARs. In our previous DOD annual reports, we showed that 4T1 cells do not express functional ß-AR (Fig. 1C,D; attached manuscript). Furthermore, NE does not alter 4T1 cellular proliferation or VEGF production *in vitro* (Fig1A,B; attached manuscript). However, up until now there has been no information regarding alpha-adrenergic receptor expression in 4T1 cells. We measured 4T1 cell α-AR signaling capacity and responsiveness to α-AR agonists *in vitro* to strengthen our contention that NE cannot directly regulate 4T1 growth through ARs.

Using *in vitro* conditions that yielded NE-mediated functional effects in other cell lines (1), we assessed functional responses to selective α-AR agonists *in vitro*. The α_1-agonist PE did not significantly alter 4T1 proliferation or VEGF production (Fig. 1E,F; attached manuscript). The α_2-agonist DEX had no effect except at the highest concentration tested (42 μM), where 4T1 proliferation was reduced and VEGF production was increased (Fig. 1G,H; attached manuscript). However, we found no evidence that the effects at high concentrations of DEX were α_2-AR-mediated. First, the K_i of DEX for α_2-AR (1.08 nM) is orders of magnitude below the effect dose of DEX. Second, yohimbine, an α_2-AR antagonist, did not block either of the DEX-induced effects (Supplemental Fig. S1A,B; attached manuscript). We also found no evidence for α_2-AR signaling via Gi protein as measured by inhibition of forskolin-induced cAMP production (Supplemental Fig. S1C; attached manuscript). It is therefore unlikely the functional effects elicited by high concentration DEX act via α_2-AR. DEX instead may stimulate imidazoline receptors that can by activated by α_2-AR agonists, but not NE (16).

Conclusions/Discussion. We conclude that NE cannot directly affect 4T1 function through α_1-, α_2- or ß-AR. Therefore, elevation of synaptic NE or stimulation of α_2-AR *in vivo* cannot alter 4T1 tumor pathogenesis by direct interactions with 4T1 tumor cells. This supports our contention that 4T1 is a model

for breast tumors that express no or low ß-AR, as described in a subset of human primary breast tumors (17). Therefore we propose that 4T1 is a good model for examining the effects of NE-induced effects on stromal cell populations in the absence of direct NE stimulation of tumor cells.

Our results demonstrated that chronic DMI treatment or α_2-AR activation with DEX increased tumor growth but the increase in tumor growth was not associated with altered angiogenesis or increased pro-angiogenic factor production (VEGF, IL-6). The next experiments were designed to explore alternative mechanisms underlying the DMI-induced increase in tumor growth.

Second harmonic generation (SHG) and collagen microstructure: Evidence for a novel mechanism underlying AR-induced alterations tumor pathogenesis

In the previous annual report, we presented evidence for a unique mechanism whereby DMI and elevated synaptic NE may augment tumor growth. This novel mechanism is based on a separate area of research in our laboratory studying tumor collagen microstructure. Multiphoton laser scanning microscopy can be employed to study tumor collagen structure using an optical technique known as second harmonic generation (SHG). SHG is an endogenous optical signal produced when two excitation photons combine to produce one emission photon, "catalyzed" by a non-centrosymmetric structure such as ordered collagen triple helices. Several factors determine SHG efficiency, all of which provide insight into collagen fiber microstructure and density by affecting SHG intensity in an image. We also quantify collagen in tumor sections by detecting collagen with standard immunofluorescence using anti-collagen type I antibodies. Results from our laboratory demonstrate an association between tumor associated macrophages, TNF-α production and altered tumor SHG emission, in the absence of changes in collagen detected with standard immunofluorescence (18). In the previous report, we showed that DMI treatment increased SHG emission intensity in the absence of changes in collagen immunofluorescence. In this report, we demonstrate alterations in tumor collagen as revealed by SHG in mice treated with DEX or ISO.

We analyzed collagen in 4T1 tumors from DMI-, DEX-, and ISO-treated mice using SHG imaging and standard immunofluorescent staining of collagen in tumor sections. **Please refer to Figure 5 in the attached manuscript for the results described in this paragraph.** SHG and immunofluorescent imaging were conducted in the same tissue section as shown in Fig. 5A. Fig. 5A shows two representative images from a 4T1 tumor of SHG-producing collagen (in blue), and collagen type I detected by standard immunofluorescence (in green). For quantifying SHG-emitting collagen, SHG-emitting pixel intensity and the percentage of pixels above threshold were measured using Image J software as described in materials and methods of the attached manuscript. Image analysis revealed that in 4T1 tumors from DMI-treated mice, the SHG pixel intensity was increased (Figure 5E) without a change in collagen pixel intensity, as measured by immunofluorescent staining of collagen (Fig. 5H). We also showed that the number of SHG pixels above a common threshold is unchanged with DMI treatment (Figure 5B). On the other hand, DEX treatment increased the number of SGH+ pixels above threshold (Figure 5C), but did not alter the intensity of SHG pixels above threshold (Figure 5F). By immunofluorescent detection, total collagen was not altered by DMI or DEX treatment (Fig. 5H,I). Figure 5K is a representative image of F4/80+ macrophages detected in a 4T1 tumor by immunofluorescent staining. Image analysis of F4/80+ macrophages revealed a slight, but non-significant, increased density of F4/80+ macrophages in DEX-treated mice (Fig. 5M, $p=0.1$), but not in DMI-treated mice (Fig. 5L). The ß-agonist ISO produced a (non-significant) increase in SHG pixel number (Fig. 5D, $p=0.07$) with no change in SHG intensity (Fig. 5G). ISO also produced a non-significant reduction in collagen pixel intensity by IHC (Fig. 5J, $p=0.15$). These alterations in SHG indicate changes in tumor collagen microstructure with DMI, DEX, and ISO treatment and each treatment uniquely correlates with augmentation of primary tumor growth (DMI) or with tumor growth and metastasis (DEX) or no alteration in tumor growth/metastasis (ISO) (see summary of these results, Table I, attached manuscript).

In the ISO-treated group, we noted the trend towards reduced collagen in Fig. 5J, an effect that was not observed with either DMI or DEX. We next determined if the effect of ISO was dependent on the region of collagen imaging within the tumor. Three regions of interest (ROIs) were taken from the geometric center (core) of the tumor or from the very edge (perimeter) of the tumor, and pixel intensity for SHG-emitting collagen and collagen detected by immunofluorescence was determined in each ROI. The results from the three ROIs for each region were averaged in every tumor. The analysis revealed that SHG-emitting collagen did not differ between saline- and ISO-treated groups independent of tumor region imaged (Fig. 9A). However, collagen detected with immunofluorescence in the center (core) of the tumor was significantly reduced in ISO-treated mice compared to saline controls (Fig. 9B). In the outer regions of the tumor (perimeter), the trend was similar, but the variability was too great to reach significance (Fig. 9B). The order index (SHG Pixel Intensity/Collagen Pixel Intensity) increased significantly in the core of tumors from the ISO-treated mice, but the increase here is due to decreased collagen, not increased SHG pixel intensity.

Conclusions/Discussion. We provide evidence here that extend our previous results demonstrating DMI-induced changes in tumor extracellular matrix collagen by measuring SHG in tumor sections. The alterations in tumor SHG-emitting and total collagen with DEX and ISO confirm our hypothesis that AR stimulation elicits alterations in tumor pathogenesis that are reflected in unique changes in the tumor extracellular microenvironment, specifically in collagen microstructure. Our laboratory has found that ablation of tumor associated macrophages or growing tumors in the absence of TNF-α alters SHG in association with altered tumor growth and metastasis. We would therefore predict elevations in macrophages and TNF-α to be associated with increased tumor progression. Here we showed no change in F4/80+ tumor associated macrophage populations with DMI treatment, but a trend toward increased F4/80+ macrophages in DEX-treated mice, along with the trends toward elevated TNF-α with DMI and DEX treatment. Furthermore, based on our results (18) associating altered SHG and increased collagen ordering with metastasis, we would have expected DMI-induced changes in SHG intensity to be associated with changes in metastasis, but DMI treatment did not alter metastasis. We speculate that the DMI-induced reduction in pro-tumor cytokines and chemokines such as RANTES and VEGF counteracted any pro-metastatic pressure elicited in part by creating an environment that differs fundamentally from the pro-tumor environment found in DEX-treated mice. We have yet to investigate alterations in collagen with salmeterol treatment. These results suggest that altered tumor collagen microstructure may be a novel mechanism whereby elevated synaptic NE may mediate changes in tumor growth through changes in the tumor extracellular matrix. .

Specific Aim 2. Determine the plasticity of sympathetic innervation following removal of blood vessels by antiangiogenic therapy and revascularization following termination of antiangiogenic therapy.

Task 3 (Months 11-15). Initiate experiments to examine impact of antiangiogenic therapy with DC101 on sympathetic innervation of breast tumors.

We attempted to purify the rat anti-VEGFR antibody DC101 and a corresponding isotype control from hybridoma supernatants. We followed a protocol used in our laboratory to purify anti-T cell hybridoma supernatants, but had no success generating the mg/ml concentrations of antibody needed for antiangiogenic therapy in mice. Therefore two alternative antiangiogenic therapies were assessed. The first is Axitinib, a small molecule tyrosine kinase inhibitor specific for the three VEGF receptors (VEGFR1, VEGFR2, VEGFR3). The second is G6-31, an anti-VEGF-A antibody that prevents human and mouse VEGF binding to VEGF receptors (19). The goal of these initial experiments was to determine if antiangiogenic therapy-induced inhibition of tumor growth and/or blood vessel density altered sympathetic innervation or activation, as measured by NE and its metabolite, normetanephrine (NMN).

Methods. BALB/c female mice were injected with $1x10^5$ 4T1 cells in a mammary fat pad. After 7 d, when tumor volume had reached 100 mm^3 on average, mice were treated IP with axitinib at 12.5 or 25 mg/kg or vehicle control once daily for 4 days. Twenty-four hours after the last injection of axitinib, mice were sacrificed and tumors were removed, weighed and processed as described above to measure NE and cytokines.

For G6-31 experiments, mice were injected with G6-31 from Genentech once tumor volume reached 100-150 mm^3 on average, as described in (19). Tumor volume was measured throughout the experiment. At sacrifice (timing varies with experiment), tumor weight, VEGF, IL-6, NE and the NE metabolite NMN were measured.

Results.
In these experiments, the primary goal was to establish a drug and therapeutic dose that inhibited 4T1 tumor growth, as not all antiangiogenic therapies inhibit 4T1 growth (20). A secondary goal was to determine if antiangiogenic therapy was associated with alterations in sympathetic neurotransmission, as measured by alterations in tumor NE or its metabolite NMN.

In the previous annual report, we showed that axitinib treatment did not alter tumor weight, tumor NE, IL-6, or VEGF. Here, we extend these negative results to demonstrate that axitinib did not significantly alter blood vessel density (Fig. 10). Tumor vessel density was assessed in the perimeter versus the core of the tumor, and the density of CD31+ vessels, as measured by the percentage of pixels above threshold, was not altered versus saline control in either region. These results suggest that axitinib did not inhibit tumor growth or reduce blood vessel density in the 4T1 tumor model.

We have also tested G6-31 as antiangiogenic therapy in 4T1 tumors. G6-31 is an anti-VEGF-A antibody that prevents human and mouse VEGF binding to VEGF receptors (19). The first experiment was designed to identify a G6-31 dose that inhibited 4T1 tumor growth. In this experiment, G6-31 injection was initiated when the tumors were on average 150 mm^3, and the mice received 4 intraperitoneal injections 3 days apart with sacrifice 3 days after the last G6-31 injection. The rate of tumor growth was reduced in mice injected with 15 mg/kg G6-31 (Fig. 11A), although at sacrifice tumor weight was significantly reduced with 1.5 mg/kg (Fig. 11B). Neither tumor NE (Fig. 11C) or NMN (Fig. 11D) were altered with antiangiogenic therapy, although trends toward reduced NE (ANOVA, $p=0.11$) and NMN (ANOVA, $p = 0.12$) were observed.

In the next experiment a dose of 10 mg/kg G6-31 was tested (to maximize the number of mice injected with our limited quantity of G6-31), and the mice were injected 5 times over a period of two weeks. Two different time points after the last injection of G6-31 were tested, day 1 and 7 to determine if effects G6-31 on sympathetic neurotransmission were dependent on time after G6-31 was discontinued.

One day after the last injection, no effect of G6-31 on the rate of tumor growth or tumor weight at sacrifice was detected, but 7 days after discontinuing G6-31, a reduced rate of tumor growth was apparent with G6-31 treatment, although tumor weight at sacrifice was not altered (Fig. 12A, B). At the 1 day time point, tumor IL-6 was significantly increased, and a non-significant trend was apparent after 7 days (Fig. 12C). VEGF was not altered by G6-31 treatment at either time point (Fig. 12D). Neither tumor NE nor NMN were altered significantly at either time point (Fig. 12 E,F).

Conclusions/Discussion. Increased tumor IL-6 was also reported by (20) in 4T1 tumors in conjunction with elevated IL-1ß with antiangiogenic therapy, and unexpectedly was associated with increased blood vessel area. Our results confirm that in 4T1, anti-angiogenic therapy elicits an increase in anti-inflammatory IL-6 and may not elicit dramatic changes in either tumor angiogenesis or tumor growth, as might be expected using other tumor models. We had predicted that (1) antiangiogenic therapy would be

associated with altered sympathetic neurotransmission and reduced blood vessel density and (2) that restoration of blood vessels after discontinuing G6-31 treatment would be associated with a return to normal sympathetic neurotransmission. The results thus far do not indicate significant impact on sympathetic neurotransmission with either antiangiogenic therapy, and the G6-31-induced increase in IL-6 did not appear to impact tumor NE/NMN. The impact of G6-31 treatment on CD31+ blood vessel density and corresponding changes in TH+ sympathetic nerve fibers have yet to be determined by immunohistochemical analysis. However, the results thus far indicate that the antiangiogenic therapy is not entirely effective at least in the aggressive 4T1 tumor model, and therefore 4T1 may not be the best tumor to use to assess interactions between blood vessels and sympathetic innervation of breast tumors.

Specific Aim 3. Determine the impact of removal of sympathetic input on the effectiveness of antiangiogenic therapy in breast tumors.

Task 4. Initiate experiments to assess impact of increased NE and sympathetic blockade with antiangiogenic therapy. (Months 15-20).

The negative results in the previous specific aim did not warrant testing this specific aim.

Specific Aim 4. Dynamically characterize the relationship between breast tumor blood vessels and sympathetic innervation *in vivo* using MPLSM.

Task 5. Back-cross TH-EGFP transgene to BALB/cByJ background (Months 1-18). This task has been completed.

Task 6. Image 4T1 blood vessels and sympathetic nerves in EGFP-TH transgenic mice with antiangiogenic therapy and cessation of therapy using MPLSM. (Months 18-24).

In the last report, images were shown of TH-EGFP nerves in excised spleen and 4T1 mammary tumors from BALB/c mice. Since then, we have also placed dorsal skinfold chambers on mice heterozygous for the transgene to image both normal skin and tumors growing in the chambers, and images from these mice are presented below.

Methods.

Multiphoton laser scanning imaging in TH-EGFP+ transgenic mice. A Spectra Physics MaiTai Ti:Sapphire laser (100 fs pulses at 80 mHz) was directed to the tissue through an Olympus BX61WI upright microscope, with beam scanning and image acquisition controlled by an Olympus Fluoview FV300 scanning system. Laser excitation wavelengths were either 840 or 905 nm as indicated in figure legends. An Olympus UMPLFL20XW water immersion objective lens (0.8 NA 20X) was used to focus excitation light and capture backward propagating fluorescent signals. Backscattered fluorophore photons were collected though the objective lens and a 603/55 nm emission filter to detect photons emitted from d-tomato (dTOM)-transfected 4T1 cells or tetramethylrhodamine (TMR)-dextran, and a 535/40 nm emission filter to detect EGFP (green). Laser power was 0.12 to 0.14 mW at the sample.

Results.

In the previous annual report, we demonstrated not only EGFP+ fiber-like structures, but EGFP+ structures with a cellular morphology during *ex vivo* imaging of excised tumors and spleens from TH-EGFP+ mice. Here we demonstrate two photon laser scanning microscopy images from dorsal skinfold chambers in wildtype and heterozygous TH-EGFP.BALB/c mice. Fig. 13A is an image from a wildtype

mouse and the blood vessels were imaged following intravenous injection with TMR-dextran with 830 nm excitation wavelength, an optimal excitation wavelength for TMR. In Fig. 13A, the blood vessels are readily apparent. In this merged image, many autofluorescent cellular structures in the green channel are apparent in these wildtype mice. Images in Fig. 13B-E were taken from TH-EGFP+ mice in which 4T1 cells were grown in dorsal skinfold chambers. Images were taken when blood vessels became apparent around the tumor. Images taken at the edge of the tumor where the blood vessels are enlarged are shown in Fig. 13B-E. At lower magnification, and at varying tissue depths (Fig. 13B, D), the large blood vessels appear to be surrounded by fluorescent structures, and at higher magnification (Fig13C,E), the fluorescence appears to be associated with fiber-like structures that may be sympathetic nerve fibers based on morphology. However, the brightness of these EGFP+ structures is no greater than the autofluorescence apparent in the wild-type mice, making it very difficult to state with assurance that this fluorescence is due to TH-EGFP transgene expression.

In an attempt to better distinguish autofluorescent cells from transgene-expressing cells, I have varied excitation wavelength, laser power, and emission filters with only limited success. For example, in Figs. 14 and 15, images taken with laser excitation wavelength of 905 nm are shown. This wavelength is optimal for EGFP, but not for TMR— the red fluorescent conjugate used to image blood vessels. Therefore, 4T1 cells transfected with the red fluorescent protein d-tomato (dTOM) were grown in a dorsal skinfold chamber implanted into a heterozygous TH-EGFP.BALB mouse in order to examine the relationship between sympathetic nerves and the tumor cells. In some regions, the tumor cells were growing in regions not associated with very little signal from the green channel, suggesting that at this wavelength autofluorescence was reduced (although at this wavelength, there was fluorescence that was apparent in both the red and green channels; see Fig. 14). In other regions of the tumor, at low magnification, dTOM-4T1 tumor cells appeared surrounded by green fluorescent structures with a mixture of morphologies (Fig. 15A). From another region of the tumor, a higher magnification image of tumor cells reveals dTOM-4T1 cells that appear to be surrounded by green fluorescent cells with a fiber-like structure, suggesting TH+ sympathetic nerve fibers (Fig. 15B). However, in another region of the tumor at a similar magnification, the distinction between TH-EGFP-expressing cells and nerve fibers based solely on morphology is not as clear (Fig. 15C).

Another way to reduce the problems associated with autofluorescence is to increase the EGFP signal. We have been conducting brother-sister pairings to develop a colony that is homozygous for the transgene. Unfortunately, the breeding has not gone as well as the cross breeding to BALB/c mice. Litters are much smaller when even one breeder is homozygous for the transgene. This tells us that mice that are homozygous for the TH-EGFP transgene do not breed well. We have concluded that the best approach will be to maintain heterozygous breeders and genotype the pups with imaging being conducted on the homozygous pups. This breeding is currently on-going.

Conclusion/Discussion. Ex vivo imaging of 4T1 tumors grown in the mammary fat pad in BALB/c mice expressing the TH-EGFP transgene revealed EGFP+ nerve fibers in the periphery of mammary tumors with a few fibers penetrating 250 μM into the tumor. However, images from wildtype mice showed distinct autofluorescent cells in both tumors and spleen. Two photon images from dorsal skinfold chambers similarly showed that is will be important to distinguish autofluorescent cells from cells expressing the EGFP-TH transgene. We conclude that at longer excitation wavelengths, autofluorescence is reduced, but it is still present and therefore work is being done to increase the EGFP signal. Furthermore, it appears that there are non-sympathetic, TH-expressing cells surrounding tumor cells, but this remains to be confirmed in homozygous with brighter EGFP signal, allowing us to better distinguish autofluorescence. Possible candidates for non-sympathetic TH-expressing cells types include macrophages (21). We continue work to identify the types of cells within and surrounding the tumor that express the TH-EGFP transgene, and to determine if these cells are capable of producing NE.

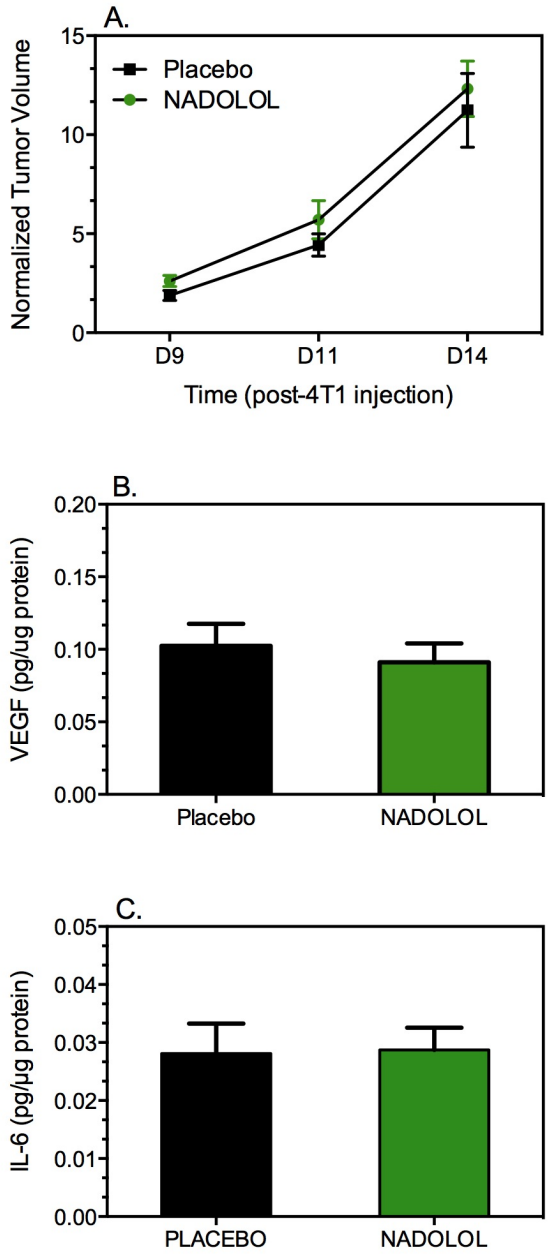

Fig. 1. Chronic ß-blockade Does Not Alter (A) Tumor Growth, (B) VEGF, or (C) IL-6 Production. Mice were implanted with pellets containing 0.5 mg nadolol (n=9) or placebo (n=9) two days prior to 4T1 inoculation. (A) Rate of tumor growth and (B) VEGF production. Results are expressed as mean ±SEM. These results are representative of experimental results from mice implanted with 5 mg nadolol.

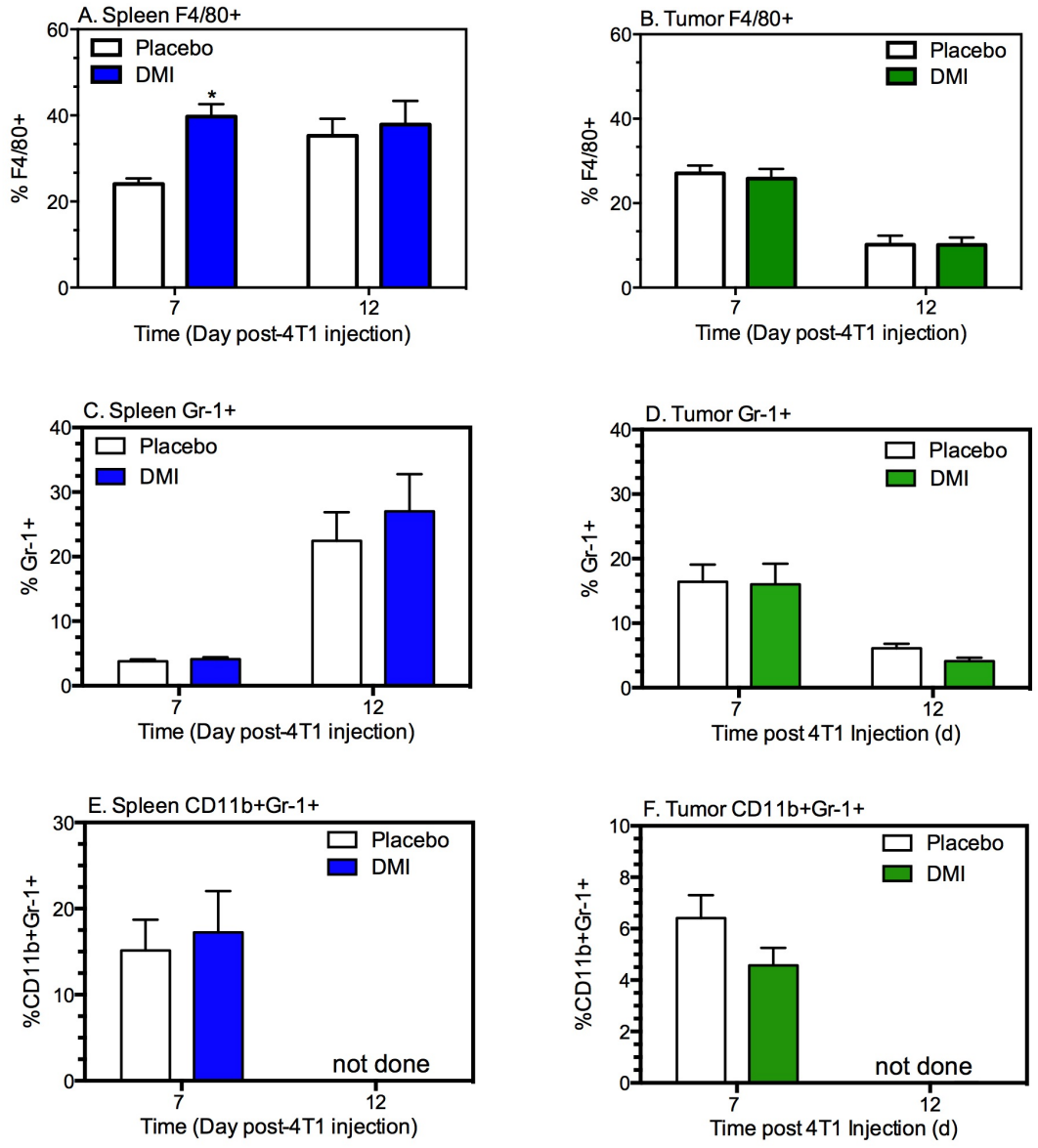

Fig. 2. Spleen and Tumor macrophage populations in DMI-treated (pellet) versus placebo mice. Spleen and tumors from mice implanted with 10 mg DMI pellets (n=5) or placebo pellets (n=6) were processed for flow cytometric analysis of F4/80+ (macrophage), CD11b+ (monocyte), Gr-1+ (neutrophil), or myeloid derived suppressor cells (CD11b+Gr-1+). All analysis was conducted on spleen and tumor cell populations based on side scatter versus forward scatter bitmap gating. Results are expressed as mean ± SEM. Statistical analysis: (A-D) Two-way ANOVA revealed significant main effects of time ($p<0.001$). In (A) main effect of time, $p=0.02$; interaction, $p=0.08$. Asterisk indicates significant difference based on Holm-Sidak's multiple comparison test ($p<0.05$).

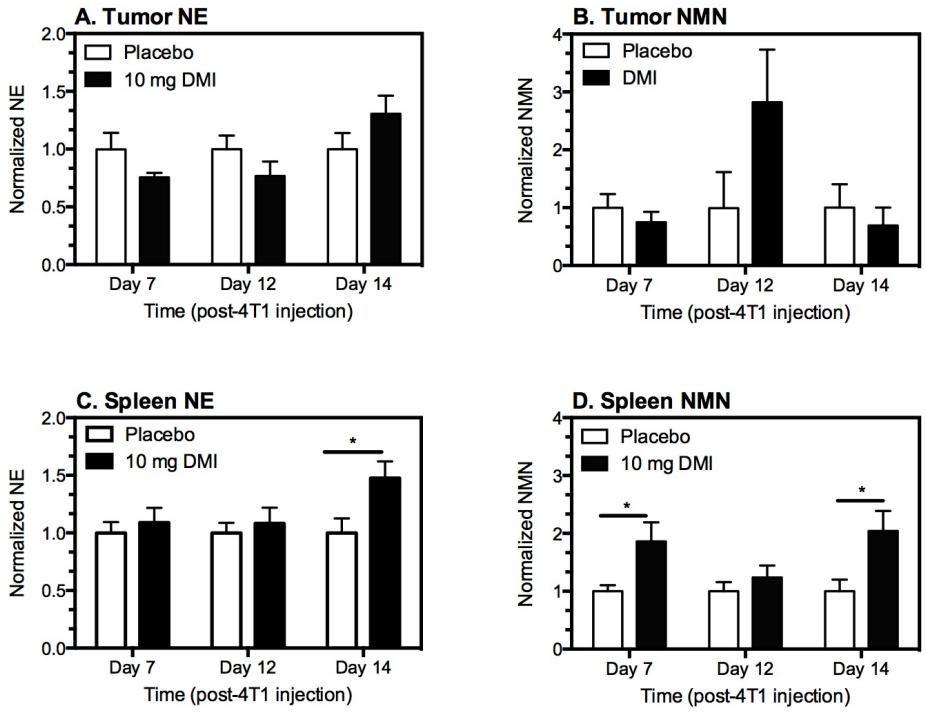

Fig. 3. Tumor and spleen NE and NMN after implantation with 10 mg DMI continuous release pellets. Placebo or DMI pellets were implanted 2 days prior to 4T1 injection. Results are expressed as the mean of the normalized response ± SEM, calculated as described in Materials and Methods under Determination of NE, NMN. (A) n=13-15 per group per time point, representing two experimental repetitions, except for at day 7 which represents the results from a single experimental repetition (n=5-6 per group). (B) Tumor NMN represents a single experimental repetition, n=5-6 per group at each time point. (C, D), n=13-15 per group per time point, representing two experimental repetitions. Statistical analyses by two-way ANOVA: (A) main effect, p= 0.7; interaction, p= 0.09; (B) main effect, p = 0.3; interaction, p= 0.08; (C) main effect, p = 0.03; interaction, p = 0.17; (D) main effect, p = 0.0007; interaction, p = 0.19. Asterisk indicates significant difference versus corresponding placebo group by Holm-Sidak's multiple comparison test, $p<0.05$.

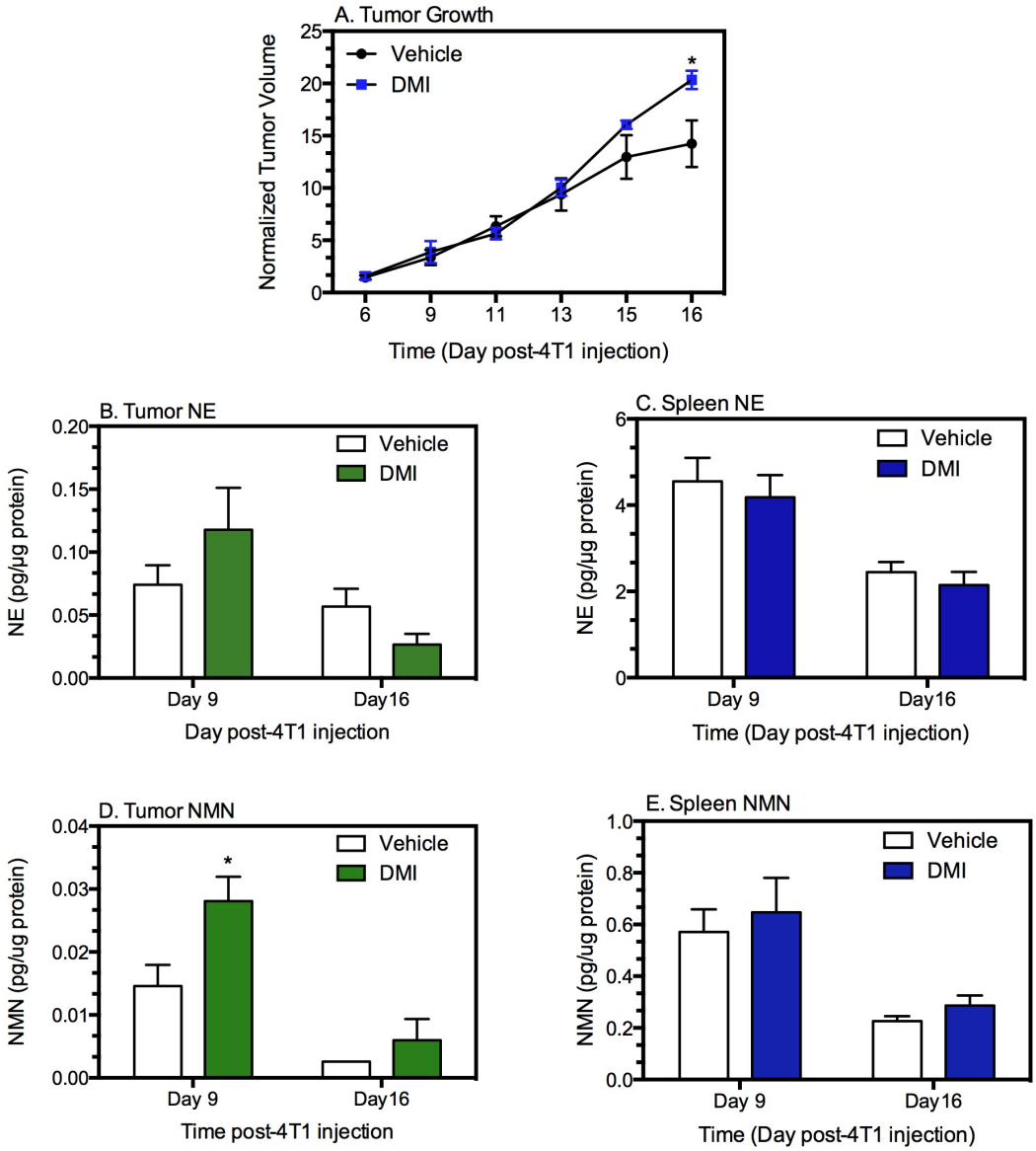

Fig. 4. Daily DMI Injections. DMI (5 mg/kg) or saline vehicle were injected daily IP beginning 2 days prior to 4T1 implantation. A. Tumor growth was measured over time in vehicle (n=4) and DMI (n=6) mice. (B) Tumor NE, (C) spleen NE, (D) tumor NMN, and (E) spleen NMN were measured 9 and 16 days post 4T1 injection (n=4 per group). Statistical analysis: (A) repeated measures 2-way ANOVA, no main effect of treatment ($p=0.3$), significant interaction ($p=0.006$), main effect of time ($p<0.0001$). (B, C, E): By two-way ANOVA, only significant effects are main effects of time ($p<0.0001$); (D): main effect of treatment, $p = 0.012$, no significant interaction, $p = 0.11$, main effect of time ($p<0.0001$). Asterisks indicate significant differences versus corresponding control by Holm-Sidak multiple comparison test, ($p<0.05$). Results are expressed as mean ± SEM.

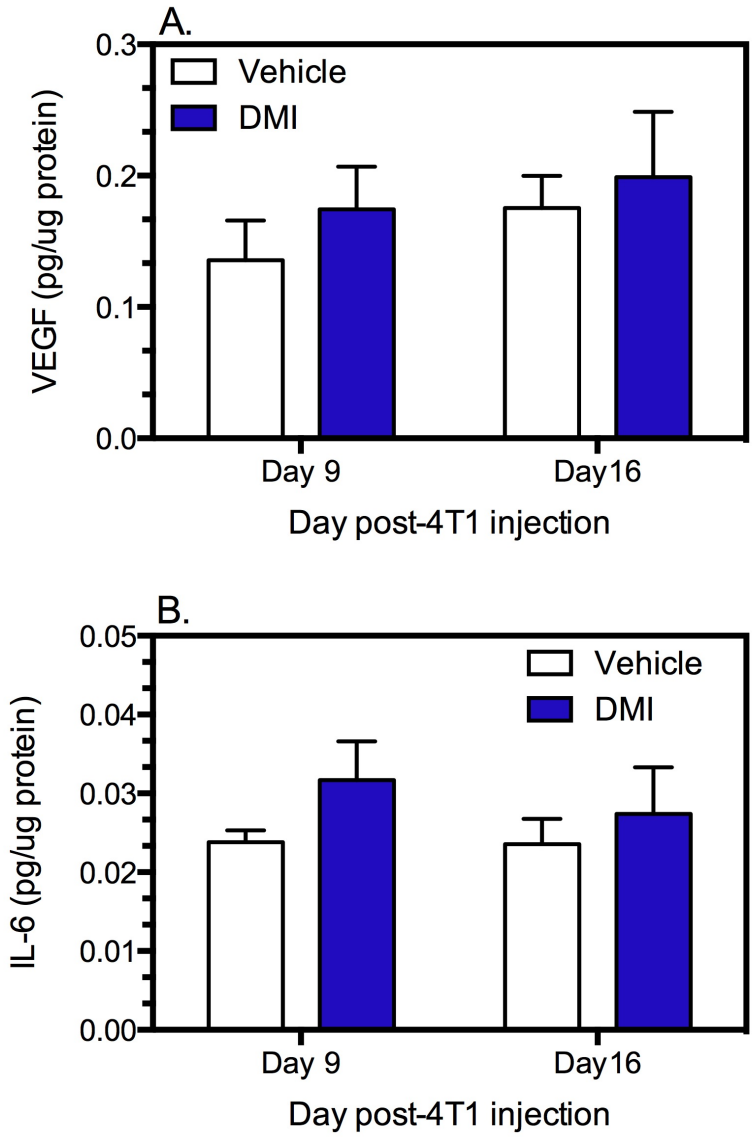

Fig. 5. Tumor Cytokine Production with Daily DMI Treatment. DMI (5 mg/kg) or saline vehicle were injected IP beginning 2 days prior to 4T1 implantation. DMI treatment (n=6) did not alter tumor (A) VEGF and (B) IL-6 day 9 or 16 post-4T1 inoculation compared to vehicle controls (n=4). Results are expressed as mean ± SEM.

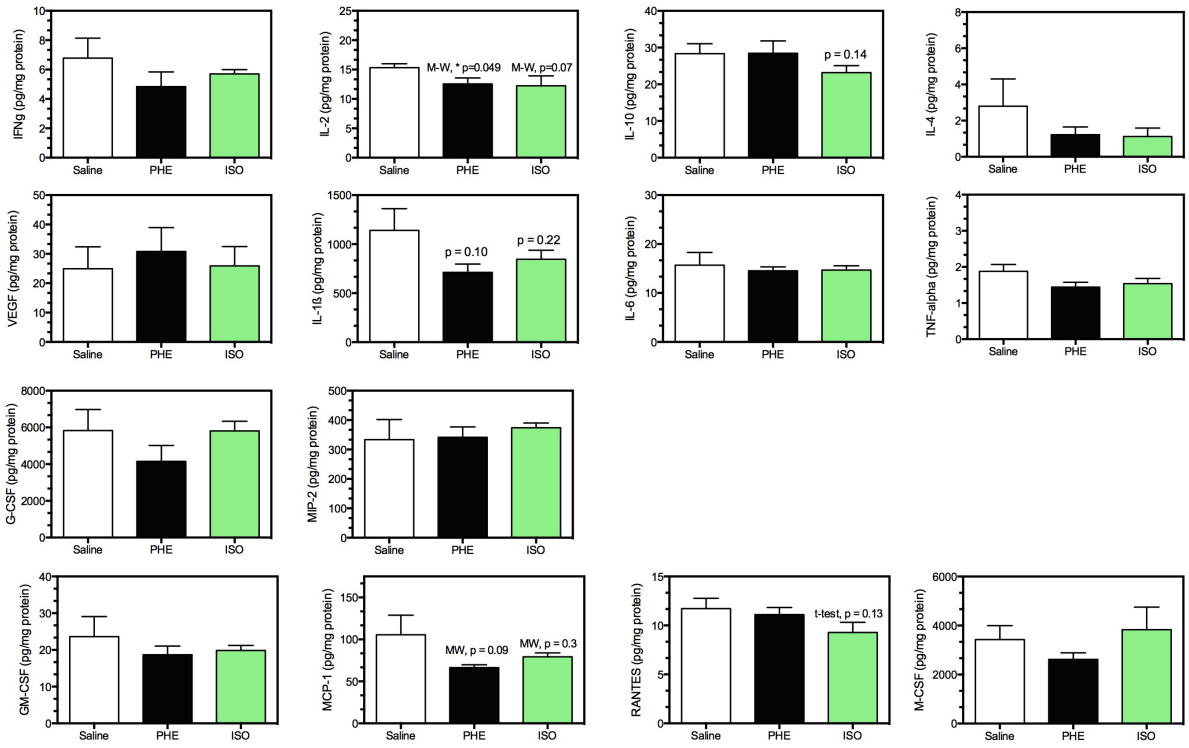

Fig. 6. Multiplex Analysis of Tumor Cytokines and Chemokines from ISO and PE-injected Mice. Daily isoproterenol (ISO) or phenylephrine (PHE) treatment was initiated 2 days prior to 4T1 injection and continued daily until sacrifice on day 19 post-4T1 injection. Results are expressed as mean ± SEM, n=6-7 per group. No statistically significant differences were detected, except for decreased IL-2 (PE group by Mann-Whitney (M-W) U test as indicated by asterisk). Trends versus saline controls are also indicated with p-values based on student's test or MW test.

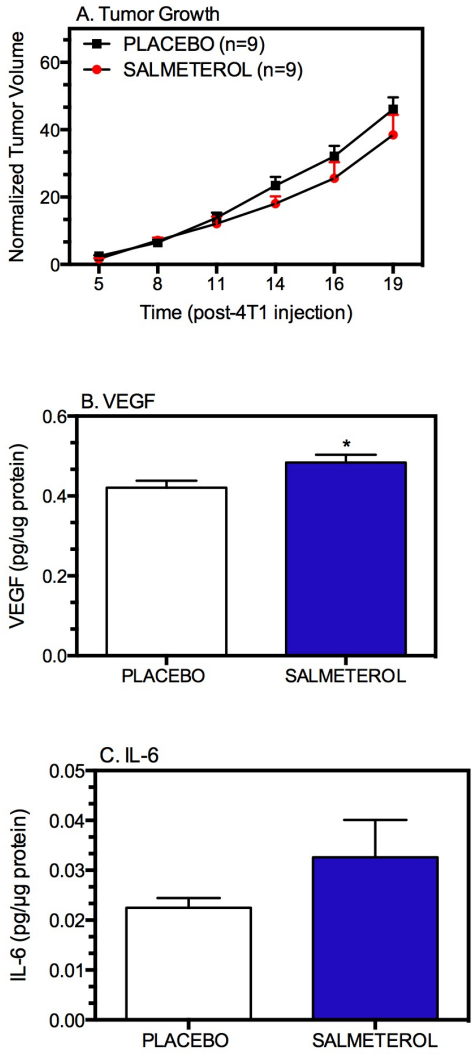

Fig. 7. Chronic salmeterol treatment did not alter tumor growth. Mice were treated with saline (n=9) or salmeterol (5 mg/kg; n=9) beginning 2 days prior to 4T1 injection, and continuing daily until sacrifice at day 19. Results are expressed as mean ±SEM. Statistical analysis: A: two-way repeated measured ANOVA, main effect of treatment, $p = 0.25$; interaction, $p=0.27$; time, $p<0.0001$; B: * Student's t-test, $p = 0.03$; C: Mann-Whitney U test, $p = 0.7$.

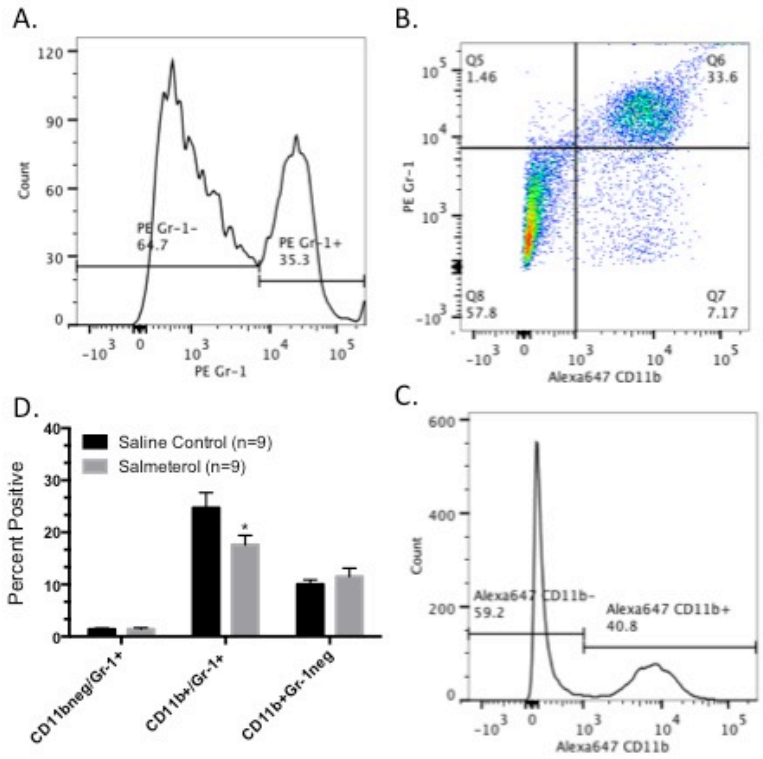

Fig. 8. Chronic salmeterol treatment reduced the frequency of myeloid suppressor (CD11b+Gr-1+) in 4T1 tumors. Mice were treated with saline or salmeterol (5 mg/kg) beginning 2 days prior to 4T1 injection, and continuing daily until sacrifice at day 14. (A,C) Representative single-color histograms of PE-anti-Gr-1+ and AlexaFluor-647-anti-CD11b+ staining of disassociated tumor cells. (B) Representative two-color histogram from the same tumor demonstrating the percentage of each subpopulation. Each histogram was obtained from gating of tumor cells by side scatter versus forward scatter. (D) The mean percent positive for each cell population in the tumor of saline- versus salmeterol-treated mice. Results are expressed as mean ± SEM. Asterisk indicates significant difference versus control by Holm-Sidak's multiple comparison test ($p<0.05$).

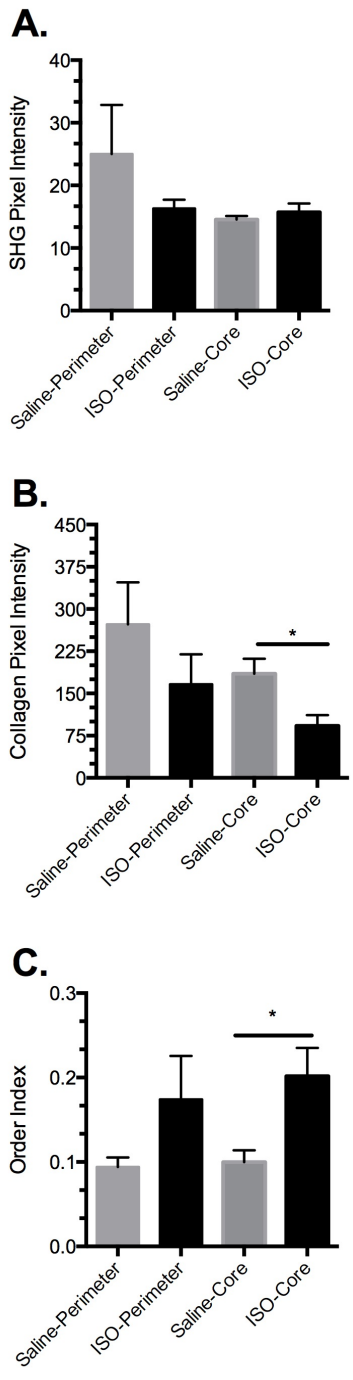

Fig. 9. **Tumor Collagen is Altered by ISO Treatment: Analysis by Tumor Region.** Tumor slices were stained for collagen by standard immunofluorescent techniques and imaged to detect collagen immunofluorescence and SHG emission with multiphoton laser scanning microscopy. For each image, ROIs were placed at three equidistant regions at the edge of the tumor (perimeter) or within the geographical center of the tumor. The pixel intensity for each ROI was calculated and averaged over the three ROIs to generate one value for the 'core' region and one value for the 'perimeter' per tumor. * indicates the two groups are significantly different by student's t-test, $p<0.05$. Results expressed as mean ± SEM, n= 6 per group.

A.

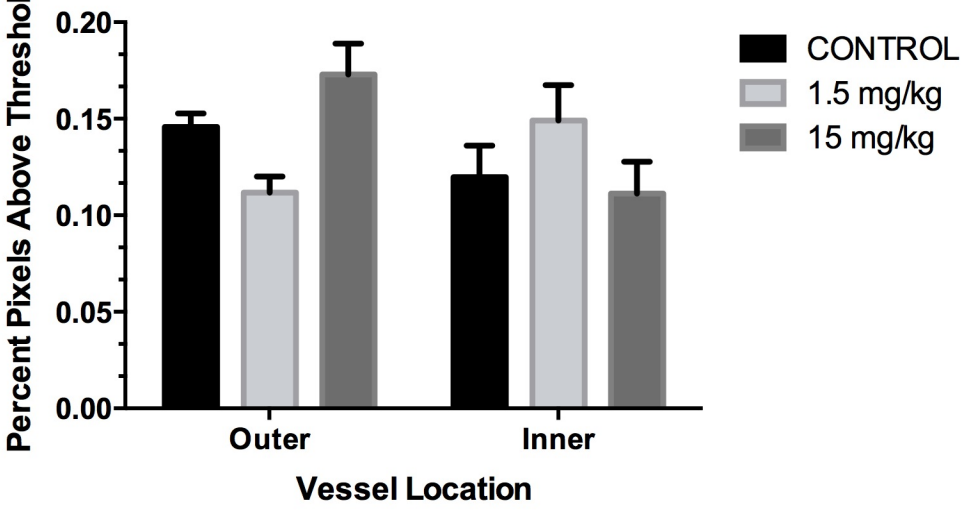

B.

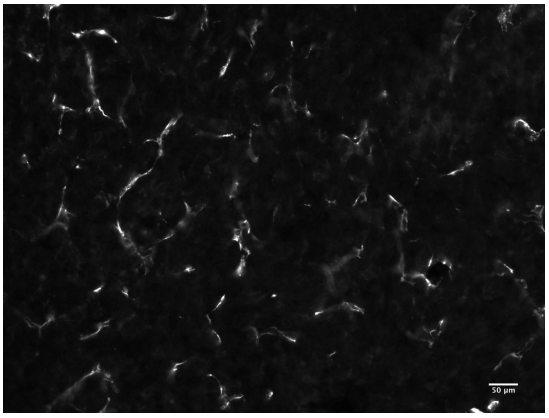

Fig. 10. Axitinib Treatment Did Not Alter CD31+ Blood Vessel Density. Axitinib treatment was begun when 4T1 mammary tumors had reached a volume of 100 mm^3 on average. Axitinib or vehicle was injected IP at the doses indicated for 4 days in a row. Mice were sacrificed one day after the last injection. A. CD31+ blood vessel density in the inner and out regions of the tumor was quantified using percent pixels above threshold. Results are expressed as mean ±SEM, n=6-7 mice per group. A representative image from the inner portion of a tumor is shown in B. Image taken using two photon laser scanning microscopy using a 20X objective lens, no electronic zoom. Scale bar = 50 µM.

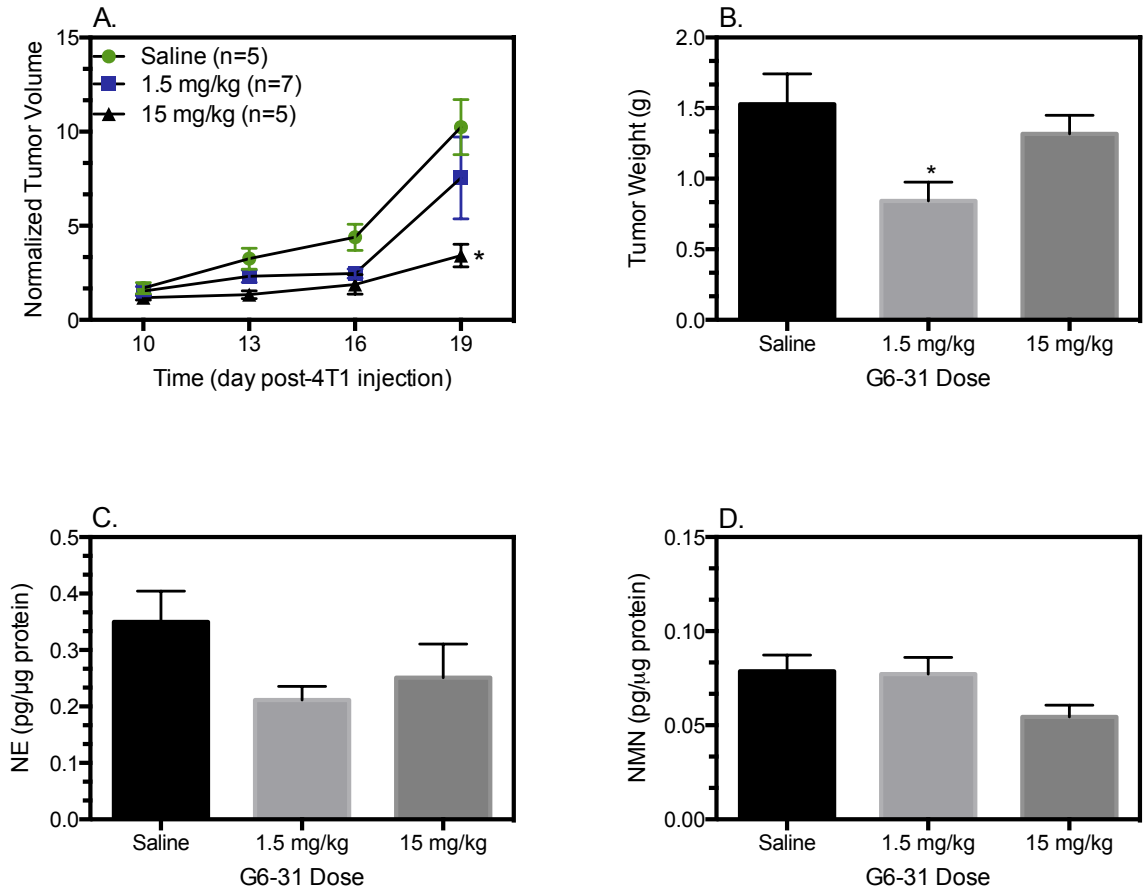

Fig. 11. 4T1 Tumor Growth and Sympathetic Neurotransmission with G6-31Antiangiogenic Therapy: 3 days after last G6-31 injection. G6-31 (1.5 mg/kg or 15 mg/kg) or saline injections were initiated when 4T1 tumors reached 150 mm^3 on average. Injections took place day 7, 10, 13, and 16 post-4T1 injection. Tumors were harvested 3 days after the last G6-31 injection, 19 days after 4T1 injection. (A) tumor growth over time, (B) tumor weight at sacrifice, (C) tumor NE concentration, (D) tumor NMN concentration. Results are expressed as mean ± SEM. In (A) repeated measures ANOVA revealed a main effect of treatment ($p = 0.02$). Asterisk in (A,B) indicates group different versus saline by Bonferroni's multiple comparison test ($p<0.05$). By one-way ANOVA, (C) $p=0.11$ and (D) $p =0.12$.

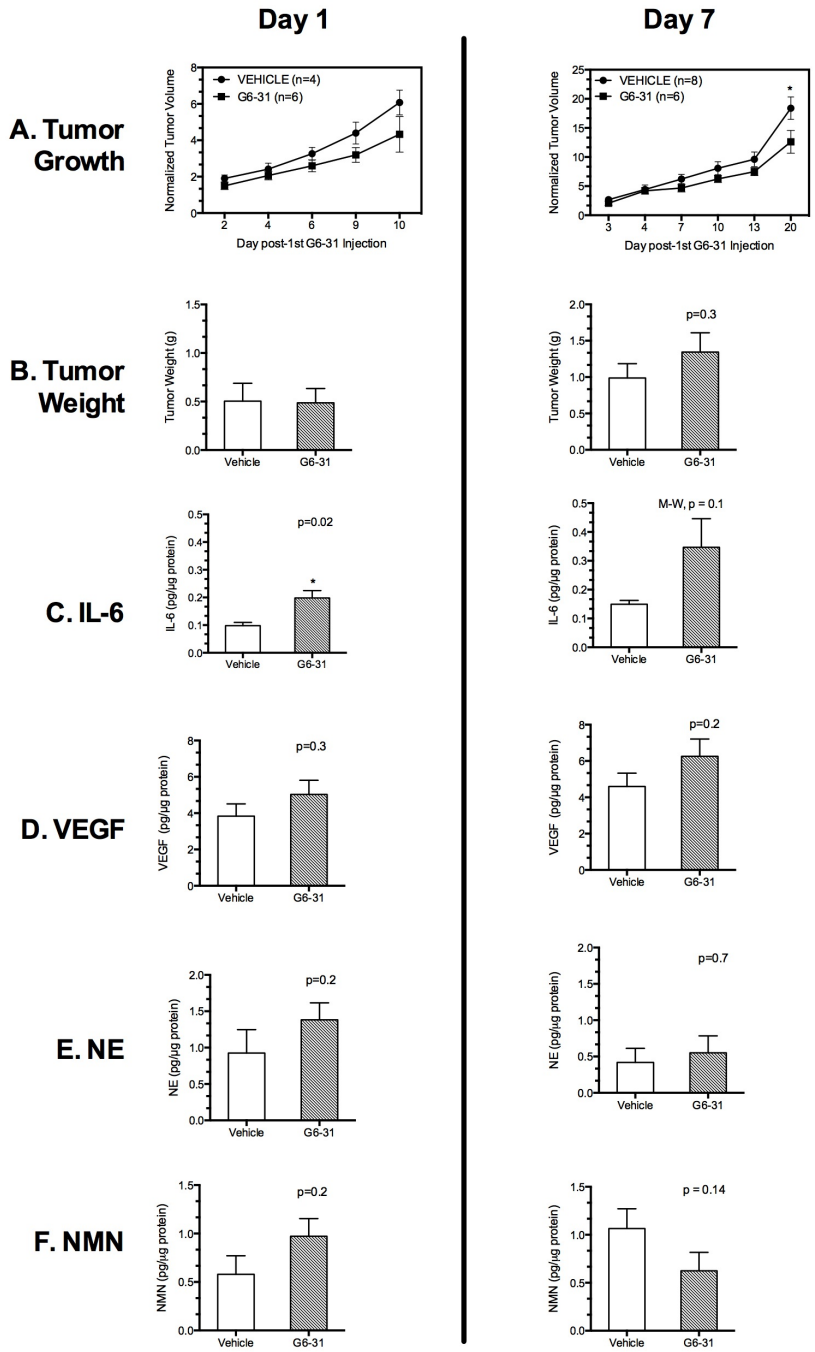

Fig. 12. Tumor Growth, Cytokine Production, and Sympathetic Neurotransmission with G6-31 Antiangiogenic Therapy. G6-31 (10 mg/kg) or saline injections were initiated when 4T1 tumors reached 150 mm^3 on average, every 2-3 days for 2 weeks. Mice were sacrificed 1 (left column) or 7 days (right column) after the last G6-31 injection. Statistical analysis: (A) Left graph: repeated measures ANOVA, effect of treatment, p = 0.18. Right graph: repeated measures ANOVA, main effect of treatment (p = 0.0014), indicated by the asterisk. In the remaining graphs, p-values from student's t-test or Mann-Whitney (M-W) U test are indicated. Significant p-values ($p \leq 0.05$) indicated by asterisk. Results are expressed as mean ± SEM. n=7 per group for 7 day; n=5 per group for 1 day experiment.

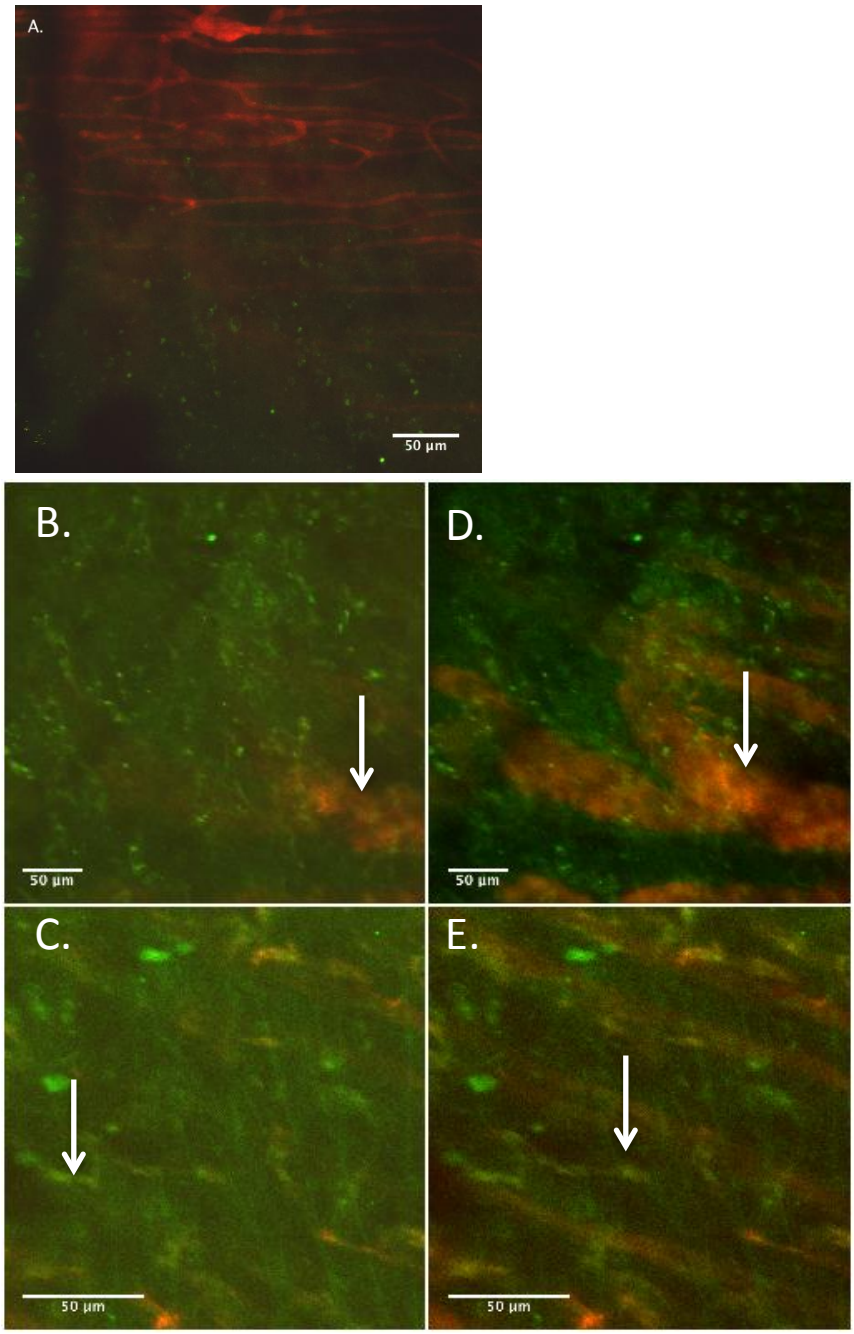
A.
50 µm
B.
50 µm
D.
50 µm
C.
50 µm
E.
50 µm

Fig. 13. Detection of TH-EGFP+ Sympathetic Nerves (green) and TMR-DEX-labeled Blood Vessels (red) by Two Photon Laser Scanning Microscopy is Confounded by Autofluorescence. Vasculature was illuminated by intravenous injection of intravenous injection of tetramethylrhodamine (TMR)- $2x10^6$ molecular weight dextran. For all images, excitation wavelength = 840 nm. (A-E) RGB merges of average intensity z projections of stacks approximately 30 µm deep with 3-µm step size. (A) Normal vasculature of the skin in a dorsal skinfold chamber implanted in a wildtype mouse. Note the autofluorescent green cells in the lower half of the image. (B-E) Images taken from a TH-EFP+ heterozygous mouse bearing a dorsal skinfold chamber implanted with a 4T1 tumor (not visible in these images). (B) Enlarged blood vessel (white arrow) at the edge of the 4T1 tumor approximately 38 µM below the skin surface. (2x electronic zoom). (D) Image is from same stack as (B) but deeper, approximately 150 µM below the skin surface, showing more of the enlarged blood vessels (white arrow). (2x electronic zoom). (C, E) Higher magnification image from same dorsal skinfold chamber as (B,D). (C) 38 µm below the surface (4x electronic zoom), (D) 150 µm below the surface (4x electronic zoom). Note the fiber-like structures readily apparent in C,E (white arrows). Scale bars = 50 µm.

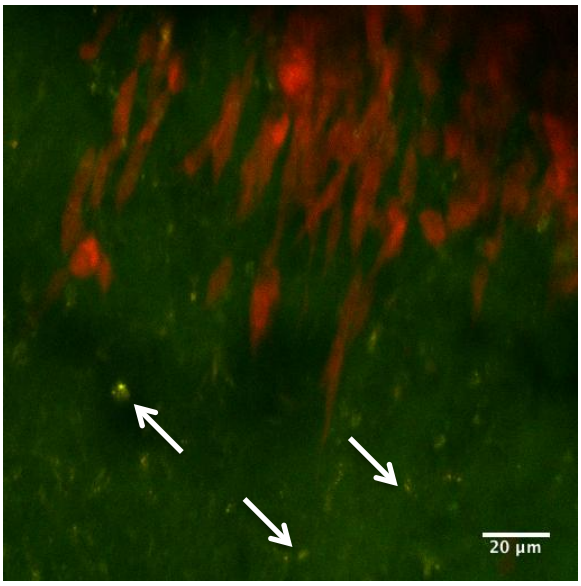

Fig. 14. 4T1 Transfected with d-tomato (dTOM)-transfected 4T1 Tumor Cells. dTOM-4T1 cells (red) growing in a dorsal skinfold chamber implanted in a heterozygous TH-EGFP.BALB/c transgenic mouse were imaged at laser excitation wavelength of 905 nm. At this wavelength, autofluorescent cells were detected as fluorescence in both the red and green channel (white arrows, cells appear yellow in this merged image). Merged image created from average intensity Z-projections, image depth = 62 µm, 3 µm step size. Electronic zoom = 2x. Scale bar = 20 µm.

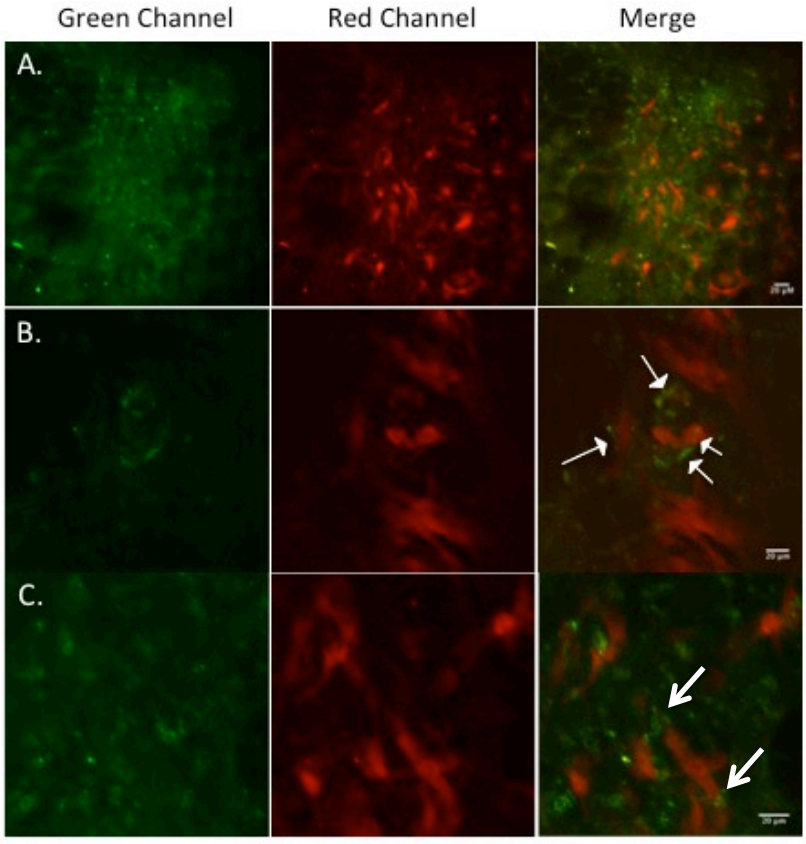

Fig. 15. EGFP-TH-expressing Cells in Close Proximity with 4T1 Transfected with d-tomato (dTOM)-transfected 4T1 Tumor Cells. dTOM-4T1 cells (red) growing in a dorsal skinfold chamber implanted in a heterozygous TH-EGFP transgenic mouse were imaged at laser excitation wavelength of 905 nm. A,B, and C are images taken from 3 distinct regions of the same tumor. Columns are images taken average intensity z-projections of stacks from the green and red channels and green/red merged. (A) 1x electronic zoom, 117 µm depth, 3 µm step size. (B) 3x electronic zoom, 14 µM depth, 1.5-µm step size. (C) 4x electronic zoom, 30 µm depth, 3 µm step size. Arrows indicate fiber like structures indicative of putative TH-EGFP+ sympathetic nerves in close proximity to dTOM-4T1 tumor cells. Scale bars = 20 µm.

KEY RESEARCH ACCOMPLISHMENTS

- Determined that most NE present in orthotopic mammary tumors is derived from sympathetic nerve terminals.
- Established that the highly metastatic murine mammary adenocarcinoma cell line 4T1 does not express functional α_1-, α_2- or ß-ARs, making 4T1 an excellent model for studying SNS regulation of tumor pathogenesis in the absence of direct sympathetic input to the tumor cells.
- Demonstrated that the SNS drives breast tumor growth in the absence of direct sympathetic input to the tumor cells.
- Demonstrated a previously undescribed role for α_2-AR activation in promoting tumor growth and metastasis.
- Demonstrated that chronic ß-AR blockade does not alter breast tumor pathogenesis under conditions of mild daily stressors.
- Established that SNS-induced tumor growth is associated with alterations in tumor fibrillar collagen microstructure as detected by second harmonic generation, suggesting a novel mechanism whereby SNS activation may regulate tumor pathogenesis.
- Demonstrated that the SNS can regulate host stromal cell populations within the tumor, specifically tumor associated macrophage populations and myeloid derived suppressor cells.
- Demonstrated that normetanephrine, a metabolite of NE, is a more sensitive measure of synaptic NE compared to measuring total NE.
- Demonstrated that two drugs that are used in humans, desipramine, a tricyclic antidepressant, and dexmedetomidine, an α_2-AR agonist used as a sedative in cancer patients, increased 4T1 tumor growth (DMI and DEX) and metastasis (DEX only).
- By multiphoton laser scanning microscopy, confirmed presence of sympathetic nerve fibers in 4T1 breast tumors grown in TH-EGFP.BALB/c mice that express enhanced green fluorescent protein in tyrosine hydroxylase expressing sympathetic nerves.

REPORTABLE OUTCOMES

PUBLISHED MANUSCRIPTS

Madden, K.S., M.J. Szpunar, E. B. Brown. 2013. Early Impact of Social Isolation and Breast Tumor Progression in Mice. Brain Behavior and Immunity. 30: S135-S141. DOI: 10.1016/j.bbi.2012.05.003 (http://dx.doi.org/10.1016/j.bbi.2012.05.003)

SUBMITTED MANUSCRIPTS

Mercedes J. Szpunar, Kathleen A. Burke, Ryan P. Dawes, Edward B. Brown, and Kelley S. Madden. The Antidepressant Desipramine and α_2-Adrenergic Receptor Activation Promote Breast Tumor Progression in Association with Altered Collagen Structure. (submitted to Cancer Prevention Research)

POSTER PRESENTATIONS:

EVIDENCE FOR SYMPATHETIC NERVOUS SYSTEM AND NOREPINEPHRINE REGULATION OF BREAST CANCER PATHOGENESIS. MJ Szpunar, KS Madden, KM Liverpool, EB Brown. 15th Annual University of Rochester Cancer Center Symposium. Rochester, NY (November 11, 2010.)

SYMPATHETIC NERVOUS SYSTEM INNERVATION AND FUNCTION IN A BETA-ADRENERGIC RECEPTOR NEGATIVE BREAST CANCER MODEL IN MOUSE. M.J. Szpunar; K.S. Madden, ; K.M. Liverpool; and E.B. Brown. Psychoneuroimmunology Research Society Annual Meeting, PNI Mechanisms of Disease: From Pathophysiology to Prevention and Treatment, June 8-11, 2011; Chicago, IL.

DETECTION OF SYMPATHETIC TYROSINE HYDROXYLASE-POSITIVE (TH+) NERVE FIBERS IN ORTHOTOPIC MAMMARY TUMORS BY MULTIPHOTON LASER SCANNING MICROSCOPY (MPLSM). K.S. Madden, M.J. Szpunar, E.M. Bouta, E.B. Brown. Psychoneuroimmunology Research Society Annual Meeting, PNI Mechanisms of Disease: From Pathophysiology to Prevention and Treatment, June 8-11, 2011; Chicago, IL.

SYMPATHETIC INNERVATION AND FUNCTION IN BREAST CANCER MODELS. M.J Szpunar, K.S. Madden, K.M. Liverpool, E.B. Brown. 2011. Department of Defense Breast Cancer Research Program Era of Hope Conference. Orlando, FL, August 2-5, 2011.

DETECTION OF SYMPATHETIC INNERVATION AND NOREPINEPHRINE IN ORTHOTOPIC AND SPONTANEOUSLY OCCURRING ANIMAL MODELS OF BREAST CANCER. K.S. Madden, M.J. Szpunar, D. Byun, K.M. Liverpool, E.B. Brown. American Association of Cancer Special Conference on Tumor Microenvironmental Complexity: Emerging Roles in Cancer Therapy, Orlando, FL, November 3-6, 2011.

EVIDENCE FOR SYMPATHETIC NERVOUS SYSTEM MODULATION OF MAMMARY TUMOR PATHOGENESIS VIA TUMOR COLLAGEN. Szpunar M.J., K.S. Madden, K.A. Burke, D.K. Byun, K.M. Liverpool, E.B. Brown. 2012. Psychoneuroimmunology Research Society Annual Meeting. Brain, Behavior, and Immunity in Health and Disease, San Diego, California, June 7-9, 2012.

DEGREES OBTAINED:

PhD awarded to Mercedes J. Szpunar in partial completion of her MD/PhD degree (6/2012). Title of Thesis: 'Evidence for Sympathetic Nervous System Regulation of Breast Cancer Progression'

FUNDING APPLIED FOR BASED ON WORK SUPPORTED BY THIS AWARD:

DOD IDEA Expansion. DOD W81XWH-12-BCRP-IDEX 'Alpha2-Adrenergic Receptors and Breast Tumor Stroma: A Novel Pathway Driving Breast Cancer Growth and Metastasis'. PI: Kelley S. Madden (Submitted 12/2012)

PERSONNEL RECEIVING PAY FROM THE RESEARCH EFFORT

Kelley S. Madden
Daniel Byun
Khawarl Liverpool
Taylor Wolfgang
Steven Lee

CONCLUSION:

We have reported here our progress in defining the role of the sympathetic nervous system in breast tumor pathogenesis using the metastatic murine 4T1 mammary tumor model. We demonstrated that the sympathetic nerves innervating 4T1 tumors are the primary source of NE. Furthermore, ablation of sympathetic nerves and the corresponding depletion of NE reduced tumor growth in association with reduced macrophages. On the other hand, elevating NE by treatment with DMI, an antidepressant that inhibits neuronal NE uptake, elevated tumor growth. We proved that DMI treatment elevated synaptic NE by measuring NE and one of its metabolites, normetanephrine in the spleen. We also showed that daily injection of DMI elevated normetanephrine in tumors, but only at a single time point. It was difficult to show consistent elevation of tumor NE or NMN with chronic DMI treatment, suggesting that elevated synaptic NE in other non-tumor sites, such as the spleen and bone marrow may be driving DMI-induced tumor growth. Combined with the relatively rapid growth of 4T1, the impact of sympathetic nerves within the tumor on tumor pathogenesis may be limited to a particular time point in the growth of the tumor.

This is an important point that will continue to be investigated in my laboratory. Despite the lack of evidence for elevated synaptic NE in tumors, DMI increased tumor growth, and the results reported here suggest that α_2-AR mediated this increase. Furthermore, α_2-AR agonist dexmedetomidine stimulated both tumor growth and metastasis, suggesting a particular potent role for selective stimulation of α_2-AR. We believe the reason DMI did not increase metastasis was related to the reduced cytokines/chemokines in DMI treated mice; these cytokines/chemokines were not altered with DEX treatment. We hypothesized that ß-AR stimulation elicited the reduced cytokines/chemokines in DMI treated mice, but ß-AR agonist treatment did not significantly reduce the cytokines/chemokines. However, the statistical trends suggested the possibility that we need to adjust timing and/or dose of the ß-AR agonists in order to prove this interesting hypothesis.

Our finding that 4T1 expresses no detectable functional ß-AR, and that 4T1 cells do not directly respond to NE, suggests that neural interactions with AR-expressing host cells, either in the tumor stroma or elsewhere in the periphery, play a central role in the 4T1 response to elevated synaptic NE. We provide evidence for a novel mechanism by which elevated synaptic NE may drive tumor pathogenesis via stromal cells. We discovered DEX- and DMI-induced alterations in extracellular matrix collagen microstructure using an endogenous optical signal, SHG. We are currently working to establish a direct functional link between the alterations in SHG intensity and altered tumor pathogenesis. We were unable to show that increased angiogenesis led to the DMI-induced increase in tumor growth, an important mechanism underlying ß-AR-induced tumor growth in ß-AR-expressing tumor models. In fact, VEGF production was transiently reduced in tumors from DMI-treated mice, although angiogenesis was not altered. These results imply that the impact of sympathetic activation on tumor pathogenesis may vary depending on breast tumor AR expression, especially AR expression by the tumor cells. These results have potential clinical implications because several studies have suggested that ß–AR blockers may be effective in the treatment of metastatic breast cancer. Furthermore, both DEX and DMI are used in clinical cancer populations. Ultimately, our goal is to apply our findings to treatment of human breast cancer and metastasis, so that safe and effective therapies that target NE and the AR can be developed.

An important goal of this grant was to investigate the relationship between sympathetic nerves and tumor blood vessels. However, we found no evidence for modulation of angiogenesis with DMI, DEX or ISO treatment. Furthermore, the anti-angiogenic treatments we tested were not as effective at inhibiting 4T1 tumor growth as we had expected. We were able to generate the EGFP-TH.BALB mice that allow us to visualize TH+ sympathetic nerves within 4T1 tumors, and we will use these mice, in combination with multiphoton laser scanning microscopy to identify potential targets cells of NE within the developing tumor. However, another tumor model should be used to test the idea of using pharmacological manipulation of sympathetic neurotransmission to promote the effectiveness of antiangiogenic therapy, preferably a tumor model in which sympathetic regulation of tumor angiogenesis has been demonstrated.

REFERENCES

1. Madden KS, Szpunar MJ, Brown EB. beta-Adrenergic receptors (beta-AR) regulate VEGF and IL-6 production by divergent pathways in high beta-AR-expressing breast cancer cell lines. Breast Cancer Res Treat. 2011;130:747-58.
2. Lorton D, Hewitt D, Bellinger DL, Felten SY, Felten DL. Noradrenergic reinnervation of the rat spleen following chemical sympathectomy with 6-hydroxydopamine: Pattern and time course of reinnervation. Brain, Behavior, and Immunity. 1990;4:198-222.
3. DuPre SA, Hunter KW, Jr. Murine mammary carcinoma 4T1 induces a leukemoid reaction with splenomegaly: association with tumor-derived growth factors. Exp Mol Pathol. 2007;82:12-24.
4. Soria G, Ben-Baruch A. The inflammatory chemokines CCL2 and CCL5 in breast cancer. Cancer Lett. 2008;267:271-85.
5. Lin EY, Nguyen AV, Russell RG, Pollard JW. Colony-stimulating factor 1 promotes progression of mammary tumors to malignancy. J Exp Med. 2001;193:727-40.
6. Eisenhofer G, Kopin IJ, Goldstein DS. Catecholamine metabolism: a contemporary view with implications for physiology and medicine. Pharmacol Rev. 2004;56:331-49.
7. Madden KS, Felten SY, Felten DL, Hardy CA, Livnat S. Sympathetic nervous system modulation of the immune system II. Induction of lymphocyte proliferation and migration in vivo by chemical sympathectomy. Journal of Neuroimmunology. 1994;49:67-75.
8. Sloan EK, Priceman SJ, Cox BF, Yu S, Pimentel MA, Tangkanangnukul V, et al. The sympathetic nervous system induces a metastatic switch in primary breast cancer. Cancer Res. 2010;70:7042-52.
9. Moore RH, Millman EE, Godines V, Hanania NA, Tran TM, Peng H, et al. Salmeterol stimulation dissociates beta2-adrenergic receptor phosphorylation and internalization. Am J Respir Cell Mol Biol. 2007;36:254-61.
10. Nagaraj S, Gabrilovich DI. Tumor escape mechanism governed by myeloid-derived suppressor cells. Cancer Res. 2008;68:2561-3.
11. Ugur F, Gulcu N, Boyaci A. Intrathecal infusion therapy with dexmedetomidine-supplemented morphine in cancer pain. Acta Anaesthesiol Scand. 2007;51:388.
12. Roberts SB, Wozencraft CP, Coyne PJ, Smith TJ. Dexmedetomidine as an adjuvant analgesic for intractable cancer pain. J Palliat Med. 2011;14:371-3.
13. Musselman DL, Somerset WI, Guo Y, Manatunga AK, Porter M, Penna S, et al. A double-blind, multicenter, parallel-group study of paroxetine, desipramine, or placebo in breast cancer patients (stages I, II, III, and IV) with major depression. J Clin Psychiatry. 2006;67:288-96.
14. Holland JC, Romano SJ, Heiligenstein JH, Tepner RG, Wilson MG. A controlled trial of fluoxetine and desipramine in depressed women with advanced cancer. Psychooncology. 1998;7:291-300.
15. Thaker PH, Han LY, Kamat AA, Arevalo JM, Takahashi R, Lu C, et al. Chronic stress promotes tumor growth and angiogenesis in a mouse model of ovarian carcinoma. Nat Med. 2006;12:939-44.
16. Khan ZP, Ferguson CN, Jones RM. alpha-2 and imidazoline receptor agonists. Their pharmacology and therapeutic role. Anaesthesia. 1999;54:146-65.
17. Powe DG, Voss MJ, Habashy HO, Zanker KS, Green AR, Ellis IO, et al. Alpha- and beta-adrenergic receptor (AR) protein expression is associated with poor clinical outcome in breast cancer: an immunohistochemical study. Breast Cancer Res Treat. 2011;130:457-63.
18. Burke R, Madden, K.S., Perry, S., Zettel, M, Brown, E.B. Tumor-associated macrophages and stromal TNF-alpha play central roles in the regulation of collagen structure in breast tumor models as visualized by second harmonic generation. submitted.
19. Fuh G, Wu P, Liang WC, Ultsch M, Lee CV, Moffat B, et al. Structure-function studies of two synthetic anti-vascular endothelial growth factor Fabs and comparison with the Avastin Fab. J Biol Chem. 2006;281:6625-31.
20. Roland CL, Lynn KD, Toombs JE, Dineen SP, Udugamasooriya DG, Brekken RA. Cytokine levels correlate with immune cell infiltration after anti-VEGF therapy in preclinical mouse models of breast cancer. PLoS One. 2009;4:e7669.
21. Dimitrijevic M, Pilipovic I, Stanojevic S, Mitic K, Radojevic K, Pesic V, et al. Chronic propranolol treatment affects expression of adrenoceptors on peritoneal macrophages and their ability to produce hydrogen peroxide and nitric oxide. J Neuroimmunol. 2009;211:56-65.

The Antidepressant Desipramine and α_2-Adrenergic Receptor Activation Promote Breast Tumor Progression in Association with Altered Collagen Structure

Mercedes J. Szpunar[a], Kathleen A. Burke[b], Ryan P. Dawes[c], Edward B. Brown[b], and Kelley S. Madden[b]*

[a] Department of Pathology, [b] Department of Biomedical Engineering, [c] Neuroscience Program, School of Medicine and Dentistry, University of Rochester, Rochester, NY USA

Running title: Norepinephrine and α_2-AR Activation Increase Tumorigenesis

Key words: Breast cancer, norepinephrine, adrenergic receptors, second harmonic generation, fibrillar collagen

Financial Support
Mercedes J Szpunar: Department of Defense Predoctoral Training Award (W81XWH-10-1-0058); Medical Scientist Training Program (NIH T32 GM07356); National Center for Research Resources (TL1 RR024135)
Kathleen A. Burke: Department of Defense Era of Hope Scholar Research Award (W81XWH-09-1-0405) to EBB
Ryan P. Dawes: NIH Training Grant in Neuroscience
Edward B. Brown: Pew Scholar in the Biomedical Sciences Award; Department of Defense Era of Hope Scholar Research Award (W81XWH-09-1-0405); National Institutes of Health Director's New Innovator Award (1 DP2 OD006501-01)
Kelley S. Madden: Department of Defense IDEA Award (W81XWH-10-01-008), National Institutes of Health (1 R21 CA152777-01)

***Corresponding Author:**
Kelley S. Madden, Ph.D.
University of Rochester Medical Center
Department of Biomedical Engineering
Goergen Hall; RC Box 270168
Rochester, NY 14627
E-mail: Kelley_Madden@urmc.rochester.edu
Telephone: 585-273-5724
Fax: 585-276-2254

Disclosure of Potential Conflicts of Interest: The authors declare no potential conflicts of interest.

Word Count: Abstract = 240; Text = 4,952
No. of figures = 5; Tables = 1

ABSTRACT

Emotional stress activates the sympathetic nervous system (SNS) and release of the neurotransmitter norepinephrine (NE) to promote breast tumor pathogenesis. We demonstrate here that the metastatic mammary adenocarcinoma cell line 4T1 does not express functional adrenergic receptors (AR), the receptors activated by NE, yet stimulation of AR altered 4T1 tumor progression *in vivo*. Chronic treatment with the antidepressant desipramine (DMI) to inhibit NE uptake increased 4T1 tumor growth, but not metastasis. Treatment with a highly-selective α_2-AR agonist, dexmedetomidine (DEX), increased tumor growth and metastasis. Neither isoproterenol, a ß-AR agonist, nor phenylephrine, an α_1-AR agonist, altered tumor growth or metastasis. Neither DMI- nor DEX-induced tumor growth was associated with increased angiogenesis. In DMI-treated mice, tumor VEGF, IL-6, and the pro-metastatic chemokines RANTES, M-CSF, and MIP-2 were reduced. Tumor collagen microstructure was examined using second harmonic generation (SHG), a non-absorptive optical scattering process to highlight fibrillar collagen. In DMI- and DEX-treated mice, but not ISO-treated mice, tumor SHG was significantly altered. These results demonstrate that α_2-AR activation can promote tumor progression in the absence of direct sympathetic input to breast tumor cells. The results also suggest that SNS activation may regulate tumor progression through alterations in the extracellular matrix, with outcome dependent on the combination of AR activated. These results underscore the complexities underlying SNS regulation of breast tumor pathogenesis, and suggest that the therapeutic use of AR blockers, tricyclic antidepressants, and AR agonists must be approached cautiously in breast cancer patients.

INTRODUCTION

In cancer patients, chronic emotional stress or other negative psychological factors, such as depression or lack of social support promote tumor growth and progression (1, 2). The sympathetic nervous system (SNS) is an important pathway by which stress can facilitate tumor growth (3-5). The SNS neurotransmitters norepinephrine (NE) and epinephrine stimulate two major classes of adrenergic receptors (AR). In animal models employing ß-AR-expressing cancer cell lines, stressor exposure or ß-AR stimulation increased tumor growth and/or metastasis in mice by multiple tumor mechanisms, such as increased tumor angiogenesis and tumor-associated macrophages (6, 7). SNS activation can also target host cells residing in metastatic sites to promote metastasis (8). These studies provide compelling evidence that NE can target AR-expressing tumor cells or host stromal cells to modulate tumor pathogenesis.

Despite progress in understanding the molecular mechanisms underlying sympathetic regulation of tumor progression, several critical questions remain. First, the role for α-AR has not been carefully examined, despite the fact that in certain types of human breast cancer, α-AR expression has been linked to poor prognosis (9). Second, variation in breast cancer cell line AR expression (10, 11) is recapitulated in human breast tumors that display heterogeneity in α- and ß-AR expression (9), and the functional consequences of such heterogeneity have yet to be systematically explored. The impact of SNS activation in tumors that express no AR is unknown. It is reasonable to assume that when breast cancer cells express no or low levels of AR, host stromal AR would be the direct targets of elevated NE. The host stromal cells that make up a tumor, including cells of the immune system, endothelial cells, and fibroblasts, express α-AR and ß-AR in healthy tissue and in tumors (7, 12, 13). We propose that SNS activation can promote tumor pathogenesis by acting on stromal cells to alter the tumor extracellular matrix.

To test this hypothesis, we have employed the multiphoton laser scanning microscope and second harmonic generation (SHG) to visualize a component of the tumor stroma, fibrillar collagen. SHG is an endogenous optical signal produced when two excitation photons combine to produce one emission photon, "catalyzed" by a non-centrosymmetric structure, such as ordered collagen triple helices (14). Tumor collagen fiber microstructure, as revealed by SHG, is of great interest because several studies have suggested that it influences tumor progression, specifically tumor metastasis. In murine breast tumor models, tumor cells can move towards blood vessels along SHG^+ fibers, moving along SHG^+ fibers more efficiently than cells moving independently (importantly, not all collagen fibers produce detectable SHG) (15). In breast cancer patient biopsies, we have shown shifts in SHG emission patterns associated with progression to more metastatic disease (16), and SHG-based tumor-associated collagen signatures are prognostic factors for disease-free survival, independent of tumor grade, size, and hormonal receptor status (17). Finally, the extent of SHG-associated tumor cell motility is correlated with metastatic ability (18, 19). Thus, SHG imaging represents a novel imaging modality to assess the impact of SNS activation on tumor extracellular matrix and explore novel stromal pathways that may be activated by NE to influence tumor progression.

We demonstrate here that 4T1, a metastatic mammary adenocarcinoma (20), lacks functional α- and β-AR, and is unable to respond to NE *in vitro*. Therefore, we propose 4T1 as an excellent model for investigating effects of SNS activation on tumors in the absence of direct sympathetic input to tumor cells. To explore the impact of elevated NE in the 4T1 tumor model, mice were treated with the NE uptake inhibitor, desipramine (DMI), a drug used clinically as an antidepressant (21, 22). We demonstrate that chronic treatment with DMI increased orthotopic 4T1 tumor growth while highly selective α_2-AR activation by treatment with dexmedetomidine

(DEX) increased tumor growth and metastasis. Both treatments were associated with altered SHG-emitting tumor collagen. These results provide evidence that activation of the SNS can promote tumor progression and metastasis through interactions with the tumor stroma, and can do so through activation of α_2-AR.

MATERIALS AND METHODS

Mice

Female BALB/cByJ mice (6-8 weeks of age; The Jackson Laboratories, Bar Harbor, ME) were housed 3-4 per cage with food and water ad libitum, and used experimentally two weeks after arrival. All animal procedures were carried out in accordance with the *National Institutes of Health Guide for the Care and Use of Laboratory Animals* and were approved by the University of Rochester Committee on Animal Resources. The University of Rochester Animal Resource is fully accredited by AAALAC International.

4T1 Cell Culture

The murine mammary adenocarcinoma cell line 4T1 was acquired from American Type Culture Collection (Manassas, VA) and grown in complete RPMI containing penicillin/streptomycin and 10% fetal calf serum. All media and media components were purchased from Gibco, Invitrogen Inc., Carlsbad, CA. Cells were used within 3 months of acquiring and/or thawing and were regularly tested for mycoplasma contamination.

In vitro culture of 4T1 cells to measure proliferation and cytokine production was described previously (10). Proliferation was assessed using CyQuant NF Proliferation Assay kit (Invitrogen) following the manufacturer's instructions. Fluorescence was detected with a 485 nm excitation filter and 530 nm emission filter using a multiwell plate reader (Biotek). For

cytokines, cell-free supernatants were harvested after 72 hours in culture and stored at -80˚C until assay by ELISA.

Drug Treatment

Drug treatments commenced two days prior to tumor cell injection and continued for the duration of the experiment. For DMI treatment, continuous release pellets (Innovative Research of America; Sarasota, FL) were implanted subcutaneously under ketamine/xylazine anesthesia (90/9 mg/kg). The AR agonists isoproterenol (ISO; Sigma-Aldrich, St. Louis, MO), phenylephrine (PE; Sigma-Aldrich), and dexmedetomidine (DEX; Pfizer, New York, NY) were dissolved in sterile saline (Baxter Healthcare Corp., Deerfield, IL), and mice were injected intraperitoneally (IP) daily for the duration of the experiment. ISO and PE doses were chosen based in part on ISO-induced increased tumor pathogenesis reported in other murine tumor models (6, 7) and on pilot toxicity studies. Two doses of DEX were tested: 10 μg/kg elicited no apparent sedative effects and 25 μg/kg elicited mild and transient anesthetic effects (slowed movements following injection that were no longer apparent one hour after injection). DMI, ISO, and PE treatment elicited early and transient decreases in body weight (≤ 10%) that recovered over time.

Tumor Implantation, Growth, and Tissue Harvest

4T1 cells ($1x10^5$ in sterile saline) were injected into the third mammary fat pad (MFP) under ketamine/xylazine anesthesia. Tumors were measured with calipers every 2-3 days without knowledge of experimental group. Mice were sacrificed by pentobarbital overdose (200 mg/kg, IP) followed by cervical dislocation to harvest tumor, spleen, and lungs. Tumors and spleens were weighed and divided. For catecholamine and cytokine analyses, tissue was immediately placed on dry ice and stored at -80°C.

Tumor volume (V) was calculated using the equation $V=1/2*length*width^2$. Tumor growth is presented either as the raw tumor volume over time or as normalized tumor growth. Normalized tumor growth was calculated by dividing an individual's tumor volume at a given time point by its volume at the earliest time point all tumors were detected (day 3 or 5 post-4T1).

NE/Normetanephrine and Cytokine Analyses

For NE and normetanephrine, tissue was homogenized in 0.01M HCl at 10% volume (ml) by tissue weight. NE and normetanephrine were determined by ELISA (Rocky Mountain Diagnostics; Colorado Springs, CO) following the manufacturer's instructions. For cytokines, tissue was homogenized in RIPA buffer containing protease inhibitors (Pierce, Rockford, IL). Cytokines were measured using mouse-specific ELISAs (R&D Systems, Minneapolis, MN) following the manufacturer's instructions.

For multiple analyte analysis, a Milliplex mouse cytokine/chemokine magnetic bead panel kit (Millipore, catalogue #MCYTOMAD-70K) was employed following the manufacturer's instructions. A Luminex 200 plate reader equipped with xPOnent software (University of Rochester Flow Cytometry Core) was used to determine median fluorescence intensity for each analyte. The concentration of each analyte was calculated using the corresponding standard curve fit to a 5-parameter logistic equation.

For all ELISAs, absorption was measured at 450 nm using a multiwell plate reader (Synergy HT, Biotek Instruments Inc, Winooski, VT). Curve fitting and sample concentration calculations were conducted with Gen5 software (Biotek). Concentrations were normalized to total protein in homogenates as determined with a BCA protein assay (Pierce).

Immunohistochemistry, Second Harmonic Generation (SHG), and Image Analysis

Tumors were fixed in 4% paraformaldehyde for 72 hours, followed by 10% sucrose and 30% sucrose for 24 hours each. Three adjacent tumor sections (20 μm thick) were collected every 100 μm. Standard immunohistochemical techniques were used to label CD31+ blood vessels using rat-anti CD31+ antibody (diluted 1:20; Abcam, Cambridge, MA), or collagen using polyclonal rabbit anti-collagen type I antibody (diluted 1:200, Abcam). Species-appropriate Alexa-Fluor-594-conjugated secondary antibodies (Invitrogen) were used to detect the primary antibodies. FITC-conjugated anti-F4/80+ antibody (Abcam) was used to detect F4/80+ macrophages in tumor slices.

For immunofluorescent and SHG imaging of collagen, tumor sections were imaged using multiphoton microscopy. Five random fields of view per tumor section were imaged by a blinded observer using an 0.8 NA 20X water immersion objective lens and electronic zoom at 1X, one section per tumor. SHG and immunofluorescence emission was collected simultaneously under constant imaging conditions in each sample, including excitation wavelength (810 nm), laser power (8 mW at the sample) and photomultiplier tube voltages. To detect immunofluorescence, fluorophore emission was collected using bandpass filters 520/40 (for FITC) and 635/30 (for Alexa-Fluor 594). SHG signal was separated from fluorescence by a 475 nm long-pass dichroic (Semrock, Rochester, NY) and detected through a bandpass 405/30 emission filter.

All images were analyzed by personnel blinded to group using custom-written algorithms in ImageJ (NIH Freeware). To quantify CD31 immunofluorescence, a threshold that excluded autofluorescence was determined in adjoining tissue sections stained with secondary antibody alone, and the percentage of pixels above threshold was calculated. Average blood vessel area was also calculated and normalized to cell density based on 4', 6-diamino-2-phenylindole (DAPI) nuclear staining. To quantify SHG and anti-collagen immunostaining, a common

threshold was determined for all samples by determining background pixels averaged from two tissue-free images from each channel. The average background intensity was subtracted from all images, then common SHG and immunostained thresholds were applied to distinguish SHG or immunostained pixels from background pixels. Two calculations were used to represent SHG or immunohistochemical (IHC) collagen signal: the percentage of pixels above threshold in each image and the average intensity of those pixels above threshold. The SHG and collagen immunostaining values from five regions of interest from each tumor section was averaged for each animal.

Lung Metastases

Lungs were fixed in 10% formalin and paraffin-embedded. Five μm-thick sections were collected every 100 μM through the entire lung. Tissue sections were stained using standard hematoxylin and eosin (H&E) techniques. Metastases were visualized using a 4X objective lens and counted in each tissue section by a blinded observer.

β-AR Expression and Intracellular cyclic AMP

A standard radioligand binding assay was used to determine specific binding of ^{125}I-cyanopindolol (NEN Radiochemicals, Waltham, MA) to whole cells to quantify β-AR expression, as described previously (10). The procedure to measure intracellular cyclic AMP was described previously (10). Cyclic AMP content was measured by ELISA (R & D Systems) following the manufacturer's instructions.

Statistical Analyses

Statistical analyses were conducted with GraphPad PRISM software with $p<0.05$ considered statistically significant. When two groups were compared, an F-test for variance was conducted to compare variance. If variance was similar, an unpaired two-tailed student's t-test

was employed. If variance differed, group comparisons were conducted using the non-parametric Mann-Whitney U-test. To compare more than two groups, one-way or two-way ANOVA was used. When variance was significantly different between groups, the non-parametric Kruskal-Wallis test was employed, with post-hoc analysis by Dunn's multiple comparison test. Tumor growth over time was analyzed using repeated measures two-way ANOVA with time post-4T1 injection as the repeated measure variable. Significant interactions or significant main effects of treatment or time were analyzed either by simple effects analysis or by Holm-Sidak multiple comparison test.

RESULTS

4T1 Tumor Cells Do Not Respond to NE *In Vitro* or Signal via AR

To determine if NE has the capacity to directly elicit functional responses from 4T1 tumor cells, 4T1 responsiveness to NE and selective AR agonists was assessed *in vitro*. NE at varying doses did not alter 4T1 proliferation (Fig. 1A) or VEGF production (Fig. 1B) under *in vitro* conditions that yielded NE-mediated functional effects in ß-AR-expressing cell lines (10). The lack of 4T1 responsiveness is consistent with the inability to detect cell surface β-AR expression by radioligand binding with the β-AR antagonist ^{125}ICYP (Fig. 1C). Furthermore, isoproterenol (ISO), a β-AR agonist, did not induce cyclic AMP above baseline (Fig. 1D). The α_1-agonist phenylephrine (PE) did not significantly alter 4T1 proliferation or VEGF production (Fig. 1E,F). The α_2-agonist DEX had no effect except at the highest concentration tested (42 μM), where 4T1 proliferation was reduced and VEGF production was non-significantly increased (Fig. 1G, H). We found no evidence that the effects at high concentrations of DEX were α_2-AR-mediated. First, the K_i of DEX for α_2-AR (1.08 nM) is orders of magnitude below

the effective dose of DEX. Second, yohimbine, an α_2-AR antagonist, did not block either of the DEX-induced effects (supplementary Fig. S1 A,B). Furthermore, there was no evidence for α_2-AR signaling via Gi protein to inhibit cyclic AMP production ((23), supplementary Fig. S1 C). These results indicate the *in vitro* effects elicited by high concentration DEX do not act via α_2AR. Instead, DEX may act on imidazoline receptors that can by activated by α_2-AR agonists (24). We conclude that NE cannot directly affect 4T1 function through α_1-, α_2- or ß-AR. We next tested if elevated synaptic NE can alter 4T1 tumor pathogenesis *in vivo*.

4T1 Tumor Growth, but Not Metastasis, is Increased by Treatment with the NE Uptake Inhibitor DMI

The tricyclic antidepressant DMI inhibits NE reuptake through the NE transporter and thereby increases synaptic NE (21, 22). Female BALB/c mice were implanted subcutaneously with 21-day continuous release pellets containing 10 mg DMI or placebo. In the spleen, DMI treatment increased NE 2-fold and the NE metabolite normetanephrine 4-fold relative to placebo, 3 days after DMI pellet implantation (supplementary Fig. S2). Normetanephrine is a measure of released NE, because the enzyme catalyzing its production from NE is located in the synapse, outside of the neuron (25). At day 3 post-DMI, spleen mass was reduced (supplementary Fig. S2 C). DMI pellets were implanted 2 days prior to 4T1 injection to ensure NE was elevated from the beginning of tumor growth, similar to the chronic pharmacological AR activation used by other investigators to demonstrate ß-AR-induced increase in tumor growth/metastasis in ß-AR-expressing tumor models (6-8).

DMI treatment increased tumor volume (mm^3) (Fig. 2A) and growth rate (volume normalized) (Fig. 2B). In DMI-treated mice sacrificed day 7, 12, and 14 post-4T1 injection,

tumor weight was significantly altered relative to placebo (Fig. 2C), and separate analysis by day revealed an increase in tumor weight at day 14 ($p<0.05$, Holm-Sidak). Despite the increase in tumor growth, metastasis to the lungs was not altered in DMI-treated mice (Fig. 2D). DMI treatment significantly reduced tumor VEGF, a key proangiogenic cytokine (Fig. 2E), and tumor IL-6, a proinflammatory cytokine with proangiogenic activity (Fig. 2F). Separate analysis of IL-6 by day revealed a significant decrease at day 7 post-4T1 ($p<0.05$, Holm-Sidak). Despite the reduction in tumor VEGF and IL-6, DMI treatment did not alter blood vessel density as measured by immunofluorescent detection of CD31+ blood vessels (supplementary Fig. S3). These results demonstrate that DMI-induced tumor growth is not associated with increased tumor angiogenesis.

α_2-AR Activation Increases Breast Tumor Growth and Metastasis

To determine if selective activation of AR can increase tumor growth, we treated mice chronically with selective AR agonists. Mice were injected daily with 5 mg/kg ISO (nonselective β-AR agonist), 10 mg/kg PE (α_1-AR) or 10 and 25 μg/kg DEX (α_2-AR) beginning two days prior to 4T1 injection and continuing until sacrifice. Daily PE and ISO, but not DEX treatment, elicited early and transient decreases in body weight (data not shown).

ISO and PE treatment were part of the same experiment and shared a saline control group, but for ease of comparison, the normalized tumor growth for ISO and PE were graphed separately. Neither ISO nor PE treatment altered normalized tumor growth (Fig. 3A,B) or tumor volume (mm^3) (data not shown). Tumor weight and metastases were not significantly altered by ISO or PE treatment (Fig. 3C,D). Tumor VEGF and IL-6 did not differ between PE or ISO treatment and saline control groups at sacrifice (Fig. 3E, F).

Daily treatment with the highly selective α_2-AR agonist DEX increased tumor volume over time. Tumor volume in mice treated with 10 µg/kg DEX was significantly increased relative to saline controls at day 19 post-4T1 injection (Fig. 3G). When tumor volume was normalized, a large main effect of treatment ($p = 0.009$) followed by simple effects analysis revealed 10 µg/kg and 25 µg/kg DEX significantly increased tumor growth compared to saline-treated controls (Fig. 3H). A non-significant increase in tumor weight at the time of sacrifice with 10 µg/kg DEX was observed (Fig. 3I; saline vs 10 µg/kg, $p = 0.095$ by student's t-test). Unlike DMI, DEX treatment (10 and 25 µg/kg) significantly increased the number of metastasis in the lung compared to saline controls (Fig. 3J). DEX treatment did not alter tumor VEGF (Fig. 3K) or IL-6 (Fig. 3L) at sacrifice. These results demonstrate increased tumor growth and metastasis elicited by activation of α_2-AR that is not associated with elevated pro-angiogenic cytokines.

Potential Cytokine/Chemokine Mechanisms Underlying DMI- and DEX-induced Tumor Pathogenesis

To further probe the mechanisms underlying differences in DMI versus DEX-induced tumor progression, additional cytokines and chemokines were measured in tumors by multiplex analysis. In DMI-treated mice, the proinflammatory cytokine TNF-α was non-significantly increased (Fig. 4A, Mann-Whitney, $p = 0.07$). A similar trend was detected in mice treated with 10 µg/kg DEX (Fig. 4B; ANOVA, $p = 0.052$), but not in PE- or ISO-treated mice data not shown). TNF-α added directly to 4T1 cells *in vitro* did not alter 4T1 proliferation *in vitro* (supplementary Fig. S4), indicating that elevated TNF-α did not directly increase 4T1 tumor growth. Furthermore, neither DMI nor DEX treatment altered the proinflammatory cytokines IL-1ß, the T cell-associated cytokines IL-2 and IFN-

γ [illegible] IL-10 (data not shown). However, DMI

treatment reduced production of several tumor chemokines that promote tumor metastasis including RANTES (CCL-5), M-CSF (CSF-1), and MIP-2 (CCL-2) (Fig. 4A). These chemokines were not altered with DEX treatment (Fig. 4B). These results demonstrate reduced tumor chemokines with DMI treatment that were not produced with selective α_2-AR stimulation.

DMI- and DEX-induced Tumor Growth is Associated with Altered SHG-Producing Tumor Collagen

Fibrillar collagen is a prevalent component of the stromal extracellular matrix in tumor. Structural alterations in fibrillar collagen are associated with cell proliferation and motility in tumors (19, 26), and are visible via SHG imaging. Preliminary results from our laboratory demonstrated that stromal TNF-α knock-out, or depletion of macrophages, reduced tumor growth and metastasis and was associated with alterations in SHG (Burke et al, unpublished). This, combined with the association between DMI- and DEX-induced tumor growth and increased tumor TNF-α led us to examine the possibility of a matrix-based mechanism underlying the increased tumor growth.

We analyzed collagen in 4T1 tumors from DMI-, DEX-, and ISO-treated mice using SHG imaging. Figure 5A shows two representative images from a 4T1 tumor of SHG-producing collagen (in blue), and collagen type I detected by standard immunohistochemistry (in green) in the same section. Image analysis revealed that in 4T1 tumors from DMI-treated mice, the SHG-emitting pixel intensity was increased (Figure 5E; $p=0.04$) without a change in the number of SHG pixels above a common threshold (Figure 5B, $p=0.3$). On the other hand, DEX treatment increased the number of pixels above threshold (Figure 5C; $p=0.04$), but did not alter the intensity of SHG pixels above threshold (Figure 5F). By IHC, total collagen was not altered by DMI or DEX treatment (Fig. 5H, I). Figure 5K is a representative image of F4/80+ macrophages

detected in a 4T1 tumor by immunofluorescent staining. Image analysis of F4/80+ macrophages revealed a slight, but non-significant, increased density of F4/80+ macrophages in DEX-treated mice (Fig. 5M), but not in DMI-treated mice (Fig. 5L). The ß-agonist ISO produced a (non-significant) increase in SHG pixel number (Fig. 5D, $p = 0.07$) with no change in SHG intensity (Fig. 5G). ISO also produced a non-significant reduction in collagen pixel intensity by IHC (Fig. 5J, $p = 0.15$). These alterations in SHG indicate changes in tumor collagen microstructure with DMI, DEX, and ISO treatment and each treatment uniquely correlates with augmentation of primary tumor growth (DMI) or with tumor growth and metastasis (DEX) or no alteration (ISO) (summarized in Table I).

DISCUSSION

AR activation by the SNS promotes tumor growth and metastasis in several animal models of cancer. Highly heterogeneous AR e□□□□□□□□□□ has been described in breast cancer cell lines and in human breast cancer, yet the functional implications of such AR heterogeneity have yet to be elucidated. We demonstrate here that the mammary adenocarcinoma cell line 4T1 lacks α-AR and β-AR expression and signaling capacity and is unable to directly respond to NE. To our knowledge, no studies have investigated the *in vivo* impact of sympathetic activation and NE stimulation on tumor pathogenesis when the tumor cells themselves cannot directly respond to NE. Doing so removes the influence of tumor ARs and thus allows us to observe effects on AR-expressing host stromal cells that may be masked when tumors are grown from AR-expressing cell lines. Under these conditions, we demonstrated that inhibition of NE uptake to elevate synaptic NE promotes 4T1 tumor growth, and α_2-AR activation can drive tumor growth and metastasis. The distinct alterations in SHG emission from tumor collagen accompanying elevated NE and AR stimulation suggests that SNS activation may modify the

tumor extracellular matrix to regulate pathogenesis. Together, these results reveal novel pathways by which SNS activation can drive tumor growth and metastasis despite the inability of the tumor cells themselves to respond to NE.

A Role for α_2-AR and Host Stromal Cells in Tumor Growth and Metastasis

The finding that DMI treatment elevated NE and increased 4T1 tumor growth is consistent with other reports demonstrating increased tumor growth and/or metastasis mediated via ß-AR activation (6, 7). However, our results differ in several important ways from these reports. The DMI- and DEX- induced tumor growth occurred in the absence of increased angiogenesis or pro-angiogenic cytokines, pro-tumor mechanisms mediated by ß-AR stimulation in the context of ß-AR-expressing tumor cells (6, 7). Furthermore, in our AR-negative tumor model, ß-AR activation with ISO treatment did not increase lung metastasis or elevate VEGF or M-CSF (also known as CSF-1), as reported by Sloan and colleagues. It is conceivable that with ß-AR-expressing tumor cells, tumor-produced CSF-1 was elevated by ß-AR stimulation, obscuring a ß-AR-induced reduction in CSF-1 from other cellular sources. These differences suggest that tumor cell ß-AR expression is a key determinant in SNS activation regulation of tumor pathogenesis. Furthermore, we propose that in the absence of direct NE input to the tumor cells, alternative AR mechanisms acting via host stromal cells determine the impact of SNS activation.

Our results are consistent with other reports of increased proliferation by α_2-AR-expressing breast tumor cell *in vitro* and increased tumor growth *in vivo* (12, 27, 28). Our results revealed that stromal α_2-AR activation leads to increased tumor growth and metastasis, independent of AR-mediated input to the tumor cells. Intriguingly, in human breast cancer, the α_{2A}-AR gene was one of 26 tumor stroma genes that together successfully predicted poor

outcome (29). One question raised by our results is why DMI treatment did not also affect metastatic outcome along with increased tumor growth. Increased synaptic NE should activate α_2-AR and thus presumably lead to increased metastasis as observed with DEX treatment. However, NE can stimulate α_1-, α_2- and ß-AR pathways, potentially resulting in opposing signals in the tumor or elsewhere in the periphery. We propose that the inability of DMI to elicit increased metastasis despite increased tumor growth was due to a combination of activated AR. This is supported by the observation that while DEX ligation of α_2-AR did not affect VEGF, IL-6, RANTES and other pro-metastatic cytokines, DMI-induced elevation of synaptic NE reduced them, presumably via other ARs and thus providing an anti-metastatic counter to the pro-metastatic effects of α_2-AR stimulation by elevated NE. This suggests that it should be possible to reduce metastasis in this model via direct stimulation of α_1-AR and/or ß-AR. While we did not detect significant effects with ISO or PE treatment on tumor growth and metastasis, in ISO-treated mice, a trend towards reduced production of these chemokines was observed at a late time point in tumor growth (data not shown), suggesting that a more detailed time course is necessary to further test this hypothesis.

We have yet to identify the stromal targets of NE and α_2-AR stimulation or their location. We confirmed that DMI treatment increased synaptic NE in the periphery by measuring increased NE and its metabolite normetanephrine in the spleen. This result implies that DMI-induced elevation of synaptic NE may target AR-expressing cells in extratumoral host tissues that play a role in tumor pathogenesis, such as spleen and bone marrow (30). Similarly DEX treatment may target the lung and the tumor to promote metastasis. DEX and DMI both are useful clinically because of their ability to cross the blood brain barrier, so it is possible that

some of our results are mediated at the level of the central nervous system, although alterations in corticosterone were not detectable in DMI-treated mice (data not shown).

A Novel Mechanism for SNS Regulation of Tumor Progression: Collagen Microstructure and SHG Imaging

Tumor stromal cells, including macrophages and fibroblasts, regulate tumor collagen structure. The SHG signal from a given segment of collagen fiber is sensitive to the amount of collagen, as well as the diameter of the fibrils that bundle together to form fibers, their spacing, and the order versus disorder in fibril packing (14, 31). Consequently, SHG intensity produces different information about collagen than immunohistochemical detection of collagen, which is sensitive to epitope availability and hence reports primarily the total amount of collagen in a given segment.

We found that tumor SHG was increased by both DMI and DEX treatment in subtly different ways, as revealed by image analysis. We propose this difference is evidence for two independent AR pathways leading to alterations in tumor collagen. In DMI-treated mice, tumor SHG pixel brightness above threshold increased without an increase in the percentage of pixels above threshold (Fig. 5E-G). An interpretation of this result is that there is no increase in production of SHG-emitting collagen (hence no increase in percentage of pixels above threshold) but that the ability of the collagen to produce SHG is itself altered (hence leading to an increase in intensity of those pixels). As discussed above, this could be an alteration in diameter of the fibrils that bundle together to form fibers, their spacing, and the order versus disorder in fibril packing; we will call this an alteration in "SHG^{+} fiber microstructure".

On the other hand, increased SHG emission from tumors from DEX-treated mice was due to an increase in the percentage of pixels above threshold without an increase in the brightness of those pixels above threshold (Fig. 5B-D). This suggests that there is more production of SHG-emitting collagen (hence an increase in the percentage of pixels above threshold), with no significant change in the microstructure (hence no increase in intensity of those pixels); we will call this an increase in "SHG^+ fiber content". DEX stimulation of α_2-AR may activate a pathway culminating in an increased SHG^+ fiber content (Fig. 5C) in association with a trend towards increased macrophages (Fig. 5M), providing a pro-growth and pro-metastatic microenvironment for the tumor cells. Note however that neither of these types of increased SHG was associated with altered *total* collagen as measured by IHC (Fig. 5H, I). Interestingly, ISO elicited a trend towards decreased collagen intensity as measured by IHC (Fig. 5J), and despite the trend toward increased SHG+ fiber content (Fig. 5D), yielded no change in tumor growth or metastasis. These results illustrate the potential power of using SHG in the 4T1 model to distinguish overlapping or opposing effects of increased NE with sympathetic activation consistent with our proposal that NE elicits effects via mixed AR signaling that can oppose each other.

Clinical Implications

An important aspect of this work is that DMI and DEX are used clinically. A retrospective study examining the clinical use of antidepressants and breast cancer development found an association between DMI and increased breast cancer risk (32), consistent with the pro-tumor growth effect of chronic DMI treatment shown here. DEX is employed as a sedative to treat cancer pain, adding urgency to delve further into the mechanisms underlying chronic DEX treatment and increased tumor growth and metastasis (33, 34). Finally, our results with DMI and elevated synaptic NE imply a balance between pro-metastatic effects of α_2-AR and anti-

metastatic ß-AR with increased NE release. If true, caution should be applied in the clinical adjuvant use of ß-blockers, as proposed by others (3, 35).

In summary, our results strongly implicate α_2-AR activation as a promoter of tumor pathogenesis in the absence of direct sympathetic input to the tumor cells. The results suggest a unique matrix-based mechanism whereby NE can facilitate breast tumor growth, through the regulation of the tumor extracellular matrix, specifically collagen microstructure. Further investigation into this mechanism is critical in part because of the possibility of using SHG imaging to detect SNS-induced alterations in the tumor matrix as a marker of a switch to a more aggressive tumor phenotype. Our results also suggest that NE can elicit directionally opposing effects within the tumor that must be carefully investigated to understand the impact of stress-induced SNS activation in a disease as molecularly heterogeneous as breast cancer.

Disclosure of Potential Conflicts of Interest

No potential conflicts of interest were disclosed.

Acknowledgements

We thank Khawarl Liverpool, Daniel Byun, Tracy Bubel, Giuseppe Arcuri, and Taylor Wolfgang for their excellent technical assistance.

Grant Support

This work was supported by Department of Defense IDEA Award (W81XWH-10-01-008) and National Institutes of Health (1 R21 CA152777-01) to KSM, Department of Defense Era of Hope Scholar Research Award (W81XWH-09-1-0405), National Institutes of Health Director's

New Innovator Award (1 DP2 OD006501-01), and Pew Scholar in the Biomedical Sciences Award to EBB, and Department of Defense Predoctoral Training Award (W81XWH-10-1-0058) to MJS. MJS is a trainee in the Medical Scientist Training Program funded by NIH T32 GM07356. RPD is a trainee in the University of Rochester Neuroscience Program supported by NIH T32. This work was made possible by predoctoral grant number TL1 RR024135 from the National Center for Research Resources, a component of the NIH, and the NIH Roadmap for Medical Research to MJS.

REFERENCES

1. Reiche EM, Nunes SO, Morimoto HK. Stress, depression, the immune system, and cancer. Lancet Oncol. 2004;5:617-25.
2. Armaiz-Pena GN, Lutgendorf SK, Cole SW, Sood AK. Neuroendocrine modulation of cancer progression. Brain Behav Immun. 2009;23:10-5.
3. Cole SW, Sood AK. Molecular pathways: Beta-adrenergic signaling in cancer. Clin Cancer Res. 2012;18:1201-6.
4. Antoni MH, Lutgendorf SK, Cole SW, Dhabhar FS, Sephton SE, McDonald PG, et al. The influence of bio-behavioural factors on tumour biology: pathways and mechanisms. Nat Rev Cancer. 2006;6:240-8.
5. Lutgendorf SK, Sood AK. Biobehavioral factors and cancer progression: physiological pathways and mechanisms. Psychosom Med. 2011;73:724-30.
6. Thaker PH, Han LY, Kamat AA, Arevalo JM, Takahashi R, Lu C, et al. Chronic stress promotes tumor growth and angiogenesis in a mouse model of ovarian carcinoma. Nat Med. 2006;12:939-44.
7. Sloan EK, Priceman SJ, Cox BF, Yu S, Pimentel MA, Tangkanangnukul V, et al. The sympathetic nervous system induces a metastatic switch in primary breast cancer. Cancer Res. 2010;70:7042-52.
8. Campbell JP, Karolak MR, Ma Y, Perrien DS, Masood-Campbell SK, Penner NL, et al. Stimulation of host bone marrow stromal cells by sympathetic nerves promotes breast cancer bone metastasis in mice. PLoS Biol. 2012;10:e1001363.
9. Powe DG, Voss MJ, Habashy HO, Zanker KS, Green AR, Ellis IO, et al. Alpha- and beta-adrenergic receptor (AR) protein expression is associated with poor clinical outcome

in breast cancer: an immunohistochemical study. Breast Cancer Res Treat. 2011;130:457-63.

10. Madden KS, Szpunar MJ, Brown EB. Beta-Adrenergic receptors (beta-AR) regulate VEGF and IL-6 production by divergent pathways in high beta-AR-expressing breast cancer cell lines. Breast Cancer Res Treat. 2011;130:747-58.

11. Vandewalle B, Revillion F, Lefebvre J. Functional beta-adrenergic receptors in breast cancer cells. J Cancer Res Clin Oncol. 1990;116:303-6.

12. Bruzzone A, Pinero CP, Rojas P, Romanato M, Gass H, Lanari C, et al. Alpha(2)-Adrenoceptors enhance cell proliferation and mammary tumor growth acting through both the stroma and the tumor cells. Curr Cancer Drug Targets. 2011;11:763-74.

13. Nance DM, Sanders VM. Autonomic innervation and regulation of the immune system (1987-2007). Brain Behav Immun. 2007;21:736-45.

14. Moreaux L, Sandre O, Charpak S, Blanchard-Desce M, Mertz J. Coherent scattering in multi-harmonic light microscopy. Biophys J. 2001;80:1568-74.

15. Sidani M, Wyckoff J, Xue C, Segall JE, Condeelis J. Probing the microenvironment of mammary tumors using multiphoton microscopy. J Mammary Gland Biol Neoplasia. 2006;11:151-63.

16. Burke K, Tang P, Brown E. Second harmonic generation reveals matrix alterations during breast tumor progression. J Biomed Opt. 2013;18:31106.

17. Conklin MW, Eickhoff JC, Riching KM, Pehlke CA, Eliceiri KW, Provenzano PP, et al. Aligned collagen is a prognostic signature for survival in human breast carcinoma. Am J Pathol. 2011;178:1221-32.

18. Wang W, Wyckoff JB, Frohlich VC, Oleynikov Y, Huttelmaier S, Zavadil J, et al. Single cell behavior in metastatic primary mammary tumors correlated with gene expression patterns revealed by molecular profiling. Cancer Res. 2002;62:6278-88.

19. Condeelis J, Segall JE. Intravital imaging of cell movement in tumours. Nat Rev Cancer. 2003;3:921-30.

20. Aslakson CJ, Miller FR. Selective events in the metastatic process defined by analysis of the sequential dissemination of subpopulations of a mouse mammary tumor. Cancer Res. 1992;52:1399-405.

21. Schildkraut JJ, Dodge GA, Logue MA. Effects of tricyclic antidepressants on the uptake and mabolism of intracisternally administered norepinephrine-H3 in rat brain. J Psychiatr Res. 1969;7:29-34.

22. Glowinski J, Axelrod J. Inhibition of Uptake of Tritiated-Noradrenaline in the Intact Rat Brain by Imipramine and Structurally Related Compounds. Nature. 1964;204:1318-9.

23. Marjamaki A, Ala-Uotila S, Luomala K, Perala M, Jansson C, Jalkanen M, et al. Stable expression of recombinant human alpha 2-adrenoceptor subtypes in two mammalian cell lines: characterization with [3H]rauwolscine binding, inhibition of adenylate cyclase and RNase protection assay. Biochim Biophys Acta. 1992;1134:169-77.

24. Khan ZP, Ferguson CN, Jones RM. alpha-2 and imidazoline receptor agonists. Their pharmacology and therapeutic role. Anaesthesia. 1999;54:146-65.

25. Eisenhofer G, Kopin IJ, Goldstein DS. Catecholamine metabolism: a contemporary view with implications for physiology and medicine. Pharmacol Rev. 2004;56:331-49.

26. Egeblad M, Rasch MG, Weaver VM. Dynamic interplay between the collagen scaffold and tumor evolution. Curr Opin Cell Biol. 2010;22:697-706.

27. Vazquez SM, Mladovan AG, Perez C, Bruzzone A, Baldi A, Luthy IA. Human breast cell lines exhibit functional alpha2-adrenoceptors. Cancer Chemother Pharmacol. 2006;58:50-61.

28. Bruzzone A, Pinero CP, Castillo LF, Sarappa MG, Rojas P, Lanari C, et al. Alpha2-adrenoceptor action on cell proliferation and mammary tumour growth in mice. Br J Pharmacol. 2008;155:494-504.

29. Finak G, Bertos N, Pepin F, Sadekova S, Souleimanova M, Zhao H, et al. Stromal gene expression predicts clinical outcome in breast cancer. Nat Med. 2008;14:518-27.

30. DuPre SA, Hunter KW, Jr. Murine mammary carcinoma 4T1 induces a leukemoid reaction with splenomegaly: association with tumor-derived growth factors. Exp Mol Pathol. 2007;82:12-24.

31. Han X, Burke RM, Zettel ML, Tang P, Brown EB. Second harmonic properties of tumor collagen: determining the structural relationship between reactive stroma and healthy stroma. Opt Express. 2008;16:1846-59.

32. Sharpe CR, Collet JP, Belzile E, Hanley JA, Boivin JF. The effects of tricyclic antidepressants on breast cancer risk. Br J Cancer. 2002;86:92-7.

33. Roberts SB, Wozencraft CP, Coyne PJ, Smith TJ. Dexmedetomidine as an adjuvant analgesic for intractable cancer pain. J Palliat Med. 2011;14:371-3.

34. Ugur F, Gulcu N, Boyaci A. Intrathecal infusion therapy with dexmedetomidine-supplemented morphine in cancer pain. Acta Anaesthesiol Scand. 2007;51:388.

35. Powe DG, Entschladen F. Targeted therapies: Using beta-blockers to inhibit breast cancer progression. Nat Rev Clin Oncol. 2011;8:511-2.

TABLE 1

Summary of DMI, DEX, and ISO-induced Tumor Matrix Alterations

Treatment	Tumor Growth	Metastasis	SHG+ Content (Intensity)	SHG+ Fibers (% Pixels)	Total Collagen (IHC)	Macrophage Density (% pixels)
DMI (mixed AR*)	Increased	No Change	Increased	No Change	No Change	No Change
DEX (α2*)	Increased	Increased	No Change	Increased	No Change	Increased
ISO (ß*)	No Change	No Change	No Change	No Change	Decreased	Not Done

* AR directly or indirectly activated by treatment

Figure Legends

Figure 1. 4T1 Cells Do Not Express Functional AR. NE does not alter 4T1 cell proliferation (A) or VEGF production (B). 4T1 cells were incubated with NE at the concentrations indicated. Results are expressed as mean ± SD of triplicate wells from a representative experiment of 2 experimental repetitions. Statistical Analyses: (A) no main effects of NE, time, or NE x time interaction; (B) no main effects of NE or NE x time interaction, main effect of time, $p < 0.0001$; (C) No specific ß-AR radioligand binding is detectable in 4T1 cells (stars). For comparison, specific binding is readily detectable with MB-231 (diamonds). (D) 4T1 cells do not produce intracellular cyclic AMP in response to the ß-AR agonist isoproterenol (ISO). By comparison, MB-231 exhibits a robust cyclic AMP response to ISO. (E, F) 4T1 cells do not respond to the α_1-AR agonist phenylephrine (PE). For both E and F, Kruskal-Wallis test, no significant effects of DEX. (G, H) 4T1 cells incubated with the selective α_2-AR agonist DEX. (G) Kruskal-Wallis test, effect of DEX ($p=0.03$, indicated by asterisk), with no significant differences versus 0 drug by Dunn's multiple comparisons test; (H) Kruskal-Wallis test, DEX treatment, $p = 0.053$ with no differences versus 0 drug by Dunn's multiple comparisons test.

Figure 2. DMI Treatment Increased Tumor Growth but not Metastasis. Mice were implanted with 10 mg DMI or placebo continuous release pellets 2 days before 4T1 inoculation. Tumor growth expressed as volume (A) or normalized (B) is increased day 12 and 14 post 4T1 injection. Results are expressed as mean ± SEM, n=6-7 mice per group for day 7 and 12, n=9-10 per group day 14 post-4T1 injection. Results represent one of two experimental replications at each time point. Results shown in (D) were measured at sacrifice, 14 days post-4T1 injection. Statistical analyses: (A) main effect of DMI treatment, $p = 0.047$; treatment x time interaction, $p < 0.0001$; main effect of time, $p < 0.0001$; (B) main effect of DMI treatment, $p = 0.0005$;

treatment x time interaction, p=0.0001, main effect of time, p<0.0001; (C) Tumor weight: main effect of DMI, p = 0.02; DMI x time interaction, p = 0.04, main effect of time, p <0.0001; (D) Lung metastasis: Student's t-test, p = 0.6; (E) VEGF: DMI treatment, p = 0.0006, no interaction or effect of time; (F) IL-6: main effect of DMI treatment, p=0.004, no DMI x time interaction, main effect of time, p = 0.0001. Asterisks indicate significant differences versus corresponding placebo control group by Holm-Sidak's multiple comparisons test (p<0.05).

Figure 3. 4T1 Tumor Growth and Metastasis in Mice Treated with ISO, PE, or DEX. Treatment was initiated 2 days prior to 4T1 injection and continued daily until sacrifice on day 19 post-4T1 injection. Results are expressed as mean ± SEM. For (A-F) ISO and PE treatment, n = 6 per group, (G-L) DEX treatment, n=9 per group. **Statistical analyses**: (A) ISO, normalized tumor volume: no main effect of treatment (p = 0.14) or interaction by time (p = 0.22), main effect of time (p<0.0001); (B) PE, normalized tumor volume: no treatment (p = 0.4) or interaction (p = 0.4), main effect of time (p<0.0001); (C-F) PE or ISO versus saline, student's t-test, p>0.05. (G) DEX, tumor volume, no main effect of treatment, p = 0.15; DEX treatment x time interaction, p = 0.005, effect of time, p <0.0001; * Holm-Sidak multiple comparison analysis of interaction, p<0.05 versus saline-treated group; (H) DEX, normalized tumor volume, main effect of treatment, p = 0.009; interaction, p<0.0001; time, p<0.0001; ** Simple effects analysis of main effect, p<0.0001 versus saline; (I) tumor weight, p= 0.17; (J) Metastasis, p= 0.03; * Holm-Sidak analysis, p<0.05 versus saline; (K) VEGF, Kruskal-Wallis, p = 0.6; (L) IL-6, p= 0.25.

Figure 4. Multiplex Analysis of Tumor Chemokines and Cytokines in mice treated with (A) DMI or (B) DEX. DMI elicited reductions in chemokines that were not observed with DEX-treatment. Results are expressed as mean ± SEM, n=7-8 mice per group. In (A) Student's t-test

or non-parametric Mann-Whitney (M-W) p-values are indicated for each chemokine/cytokine. In (B), p-values represent analysis by one-way ANOVA. * indicates significant differences versus corresponding control group ($p<0.05$).

Figure 5. **Tumor Collagen Structure is Differentially Altered by DMI and DEX Treatment.** Tumor slices were stained for collagen by standard immunohistochemical techniques and imaged to detect immunofluorescent and SHG emission by multiphoton microscopy. Image analysis was conducted with Image J as described in materials and methods. (A) Two representative pseudo-colored images of SHG (blue) versus collagen type I (green) from a 4T1 tumor. Scale bars = 100 μm. (B, C, D) Percentage of SHG pixels above threshold; (E, F, G) SHG pixel intensity above theshold; (H, I, J) Anti-collagen immunohistochemical analysis; (K) Representative image of F4/80+ macrophages in a 4T1 tumor section by immunofluorescence. Scale bar = 100 μm. (L, M) F4/80+ immunofluorescent analysis, number of pixels above threshold. Results shown are mean ± SEM, n= 8-9 mice per group for both DMI and DEX experiments; n=6 per groups for ISO experiment. Asterisk indicates significant differences based on student's t-test, $p<0.05$ versus placebo or saline by student's t-test; M-W = Mann-Whitney non-parametric U-test.

Fig. 1

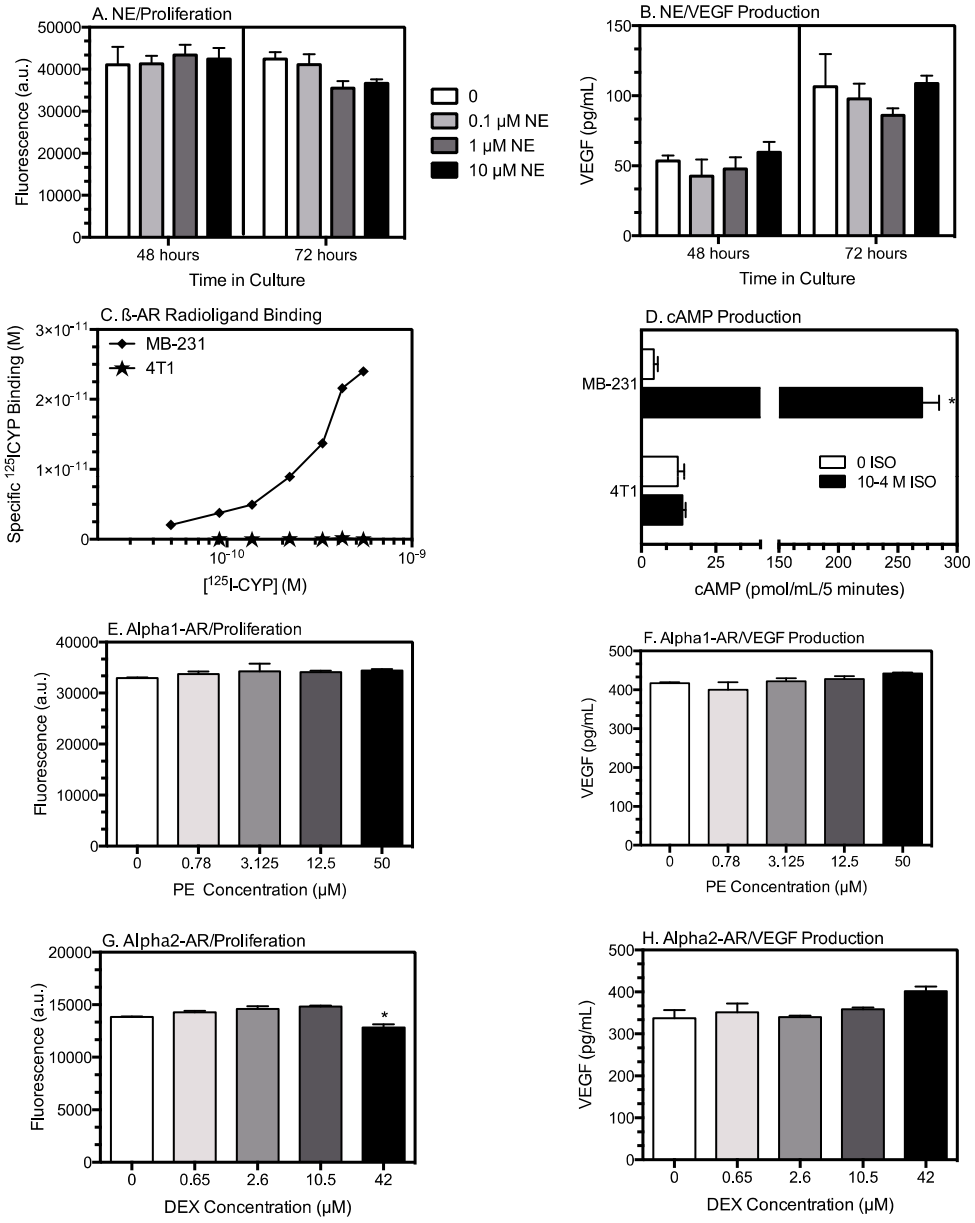
A. NE/Proliferation
Fluorescence (a.u.)
50000
40000
30000
20000
10000
0
48 hours
72 hours
Time in Culture
0
0.1 µM NE
1 µM NE
10 µM NE
B. NE/VEGF Production
VEGF (pg/mL)
150
100
50
0
48 hours
72 hours
Time in Culture
C. ß-AR Radioligand Binding
Specific [125]CYP Binding (M)
3×10-11
2×10-11
1×10-11
0
MB-231
4T1
10-10
10-9
[125I-CYP] (M)
D. cAMP Production
MB-231
4T1
*
0 ISO
10-4 M ISO
0
25
150
200
250
300
cAMP (pmol/mL/5 minutes)
E. Alpha1-AR/Proliferation
Fluorescence (a.u.)
40000
30000
20000
10000
0
0
0.78
3.125
12.5
50
PE Concentration (µM)
F. Alpha1-AR/VEGF Production
VEGF (pg/mL)
500
400
300
200
100
0
0
0.78
3.125
12.5
50
PE Concentration (µM)
G. Alpha2-AR/Proliferation
Fluorescence (a.u.)
20000
15000
10000
5000
0
*
0
0.65
2.6
10.5
42
DEX Concentration (µM)
H. Alpha2-AR/VEGF Production
VEGF (pg/mL)
500
400
300
200
100
0
0
0.65
2.6
10.5
42
DEX Concentration (µM)

Figure 2

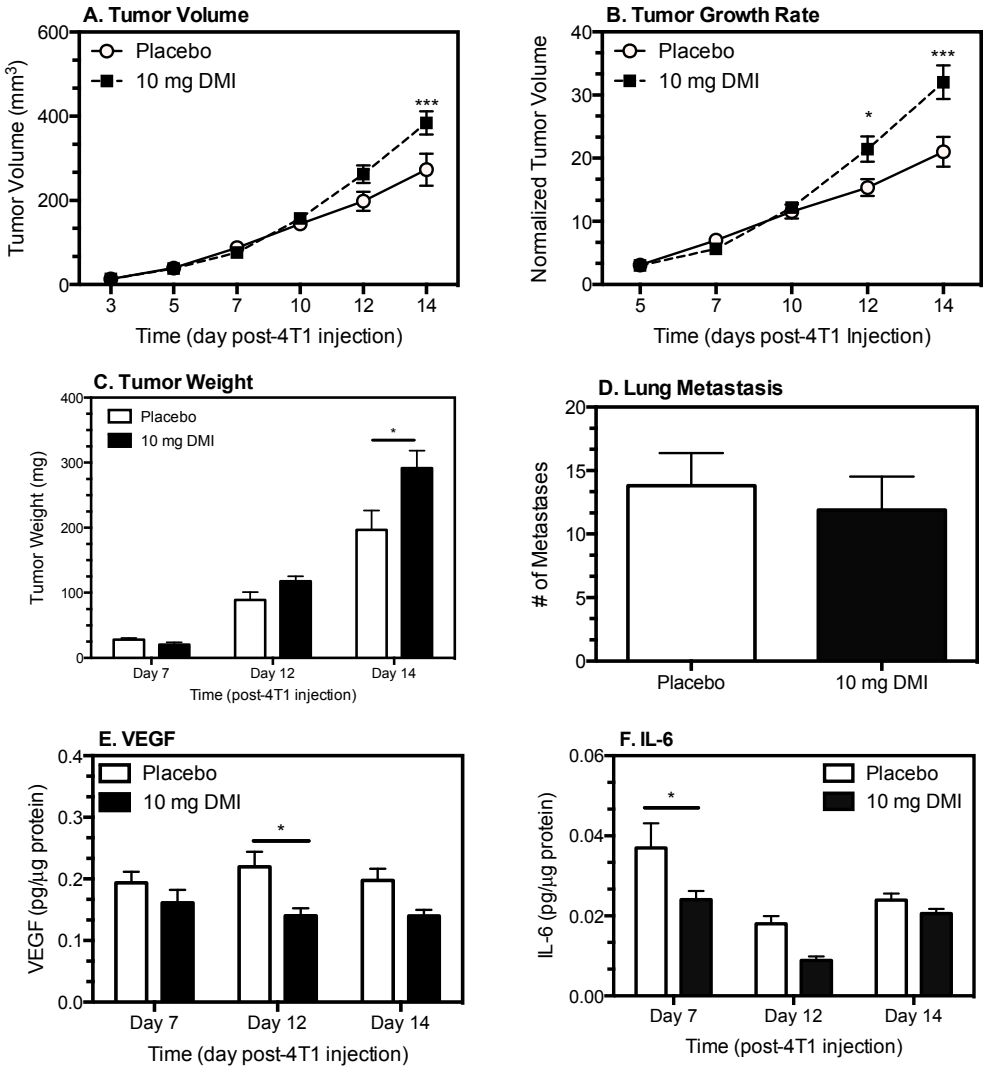
A. Tumor Volume
Placebo
10 mg DMI
Tumor Volume (mm3)
Time (day post-4T1 injection)
B. Tumor Growth Rate
Normalized Tumor Volume
Time (days post-4T1 Injection)
C. Tumor Weight
Tumor Weight (mg)
Day 7
Day 12
Day 14
Time (post-4T1 injection)
D. Lung Metastasis
# of Metastases
E. VEGF
VEGF (pg/µg protein)
Time (day post-4T1 injection)
F. IL-6
IL-6 (pg/µg protein)
Time (post-4T1 injection)

Figure 3

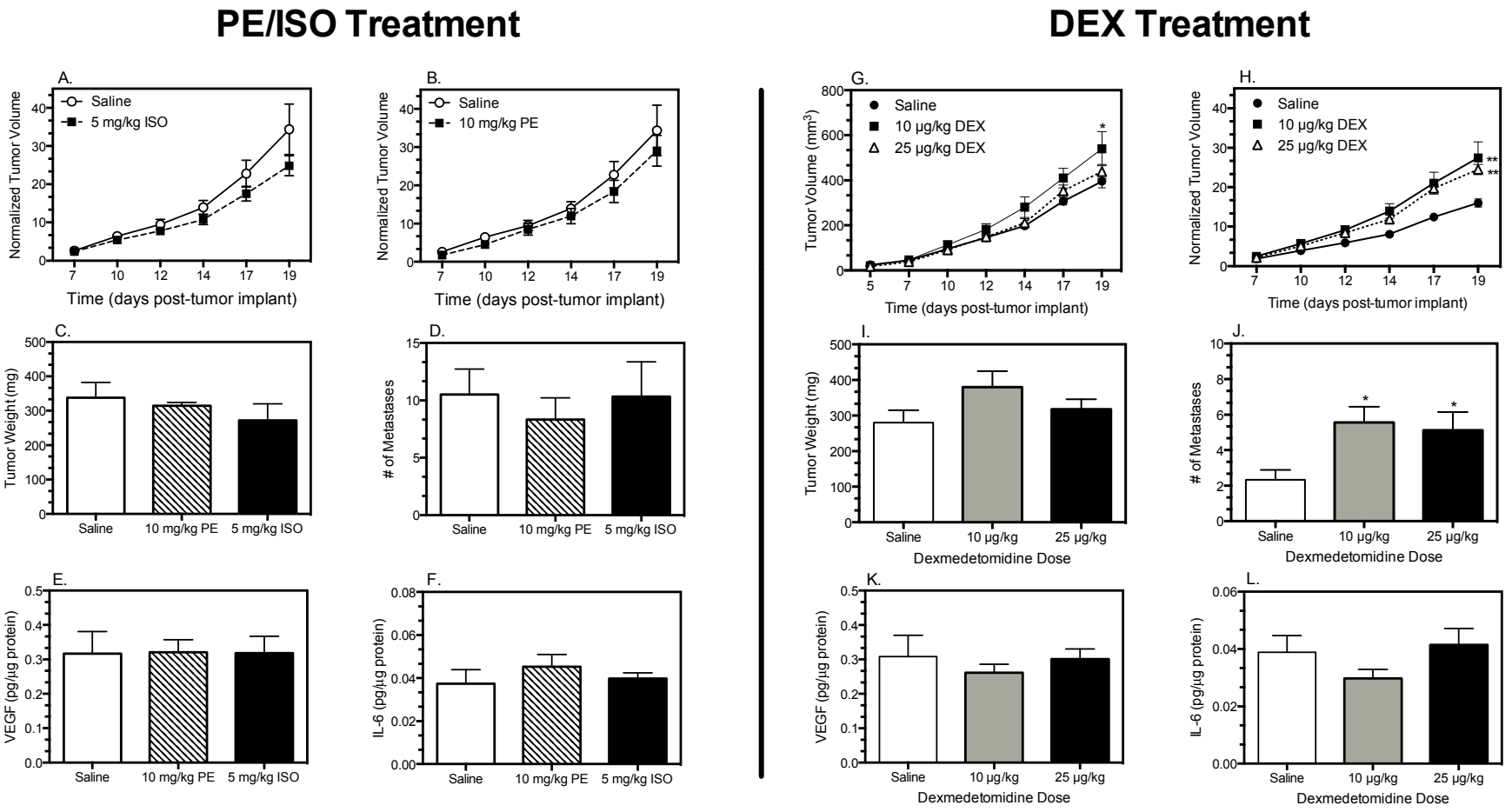
PE/ISO Treatment
DEX Treatment
A.
Saline
5 mg/kg ISO
Normalized Tumor Volume
Time (days post-tumor implant)
B.
Saline
10 mg/kg PE
Normalized Tumor Volume
Time (days post-tumor implant)
C.
Tumor Weight (mg)
Saline
10 mg/kg PE
5 mg/kg ISO
D.
# of Metastases
Saline
10 mg/kg PE
5 mg/kg ISO
E.
VEGF (pg/µg protein)
Saline
10 mg/kg PE
5 mg/kg ISO
F.
IL-6 (pg/µg protein)
Saline
10 mg/kg PE
5 mg/kg ISO
G.
Saline
10 µg/kg DEX
25 µg/kg DEX
Tumor Volume (mm3)
Time (days post-tumor implant)
H.
Saline
10 µg/kg DEX
25 µg/kg DEX
Normalized Tumor Volume
Time (days post-tumor implant)
I.
Tumor Weight (mg)
Saline
10 µg/kg
25 µg/kg
Dexmedetomidine Dose
J.
# of Metastases
Saline
10 µg/kg
25 µg/kg
Dexmedetomidine Dose
K.
VEGF (pg/µg protein)
Saline
10 µg/kg
25 µg/kg
Dexmedetomidine Dose
L.
IL-6 (pg/µg protein)
Saline
10 µg/kg
25 µg/kg
Dexmedetomidine Dose

Figure 4

A. DMI Treatment

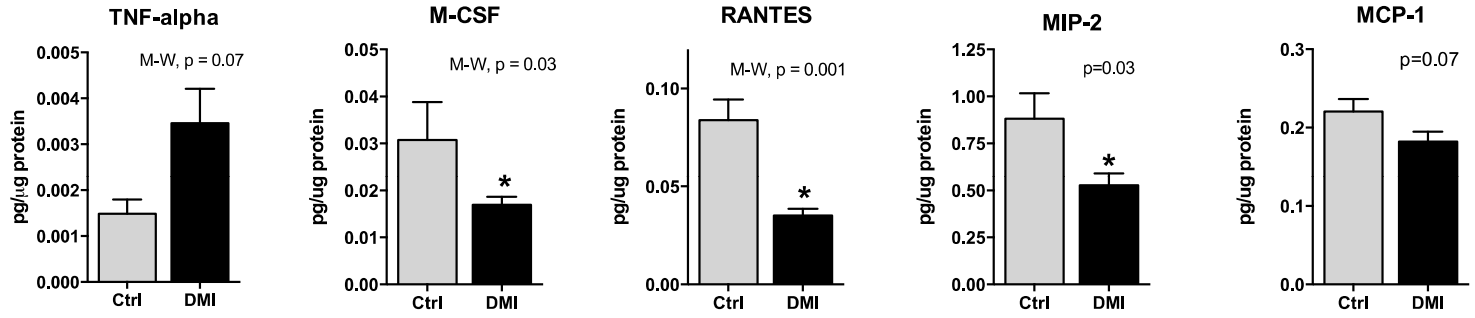

B. DEX Treatment

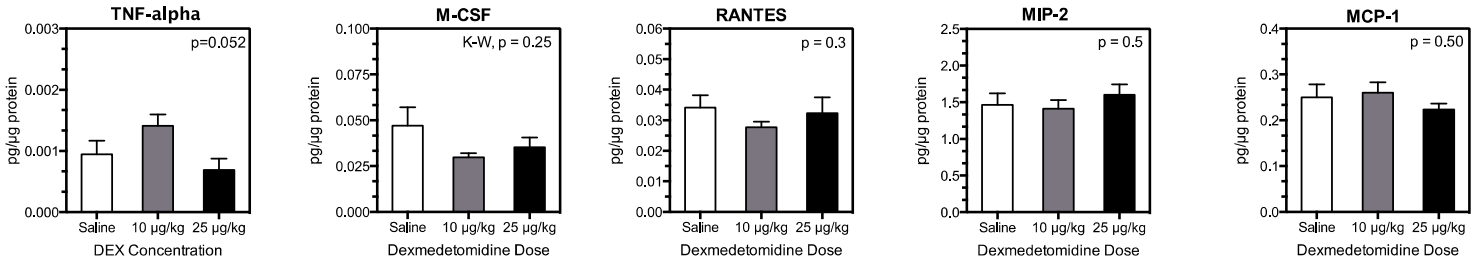

Fig. 5 SHG

A. SHG/Collagen Overlay

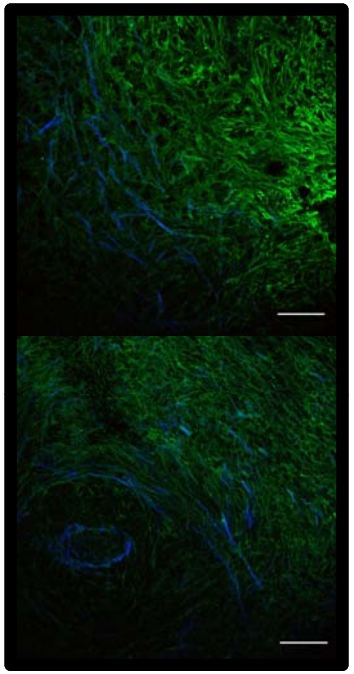

K. F4/80+ Macrophages

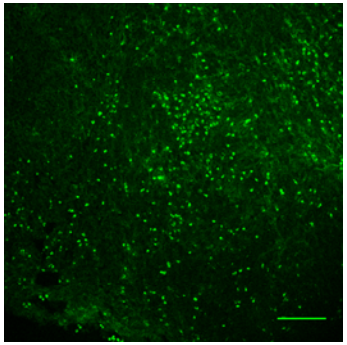

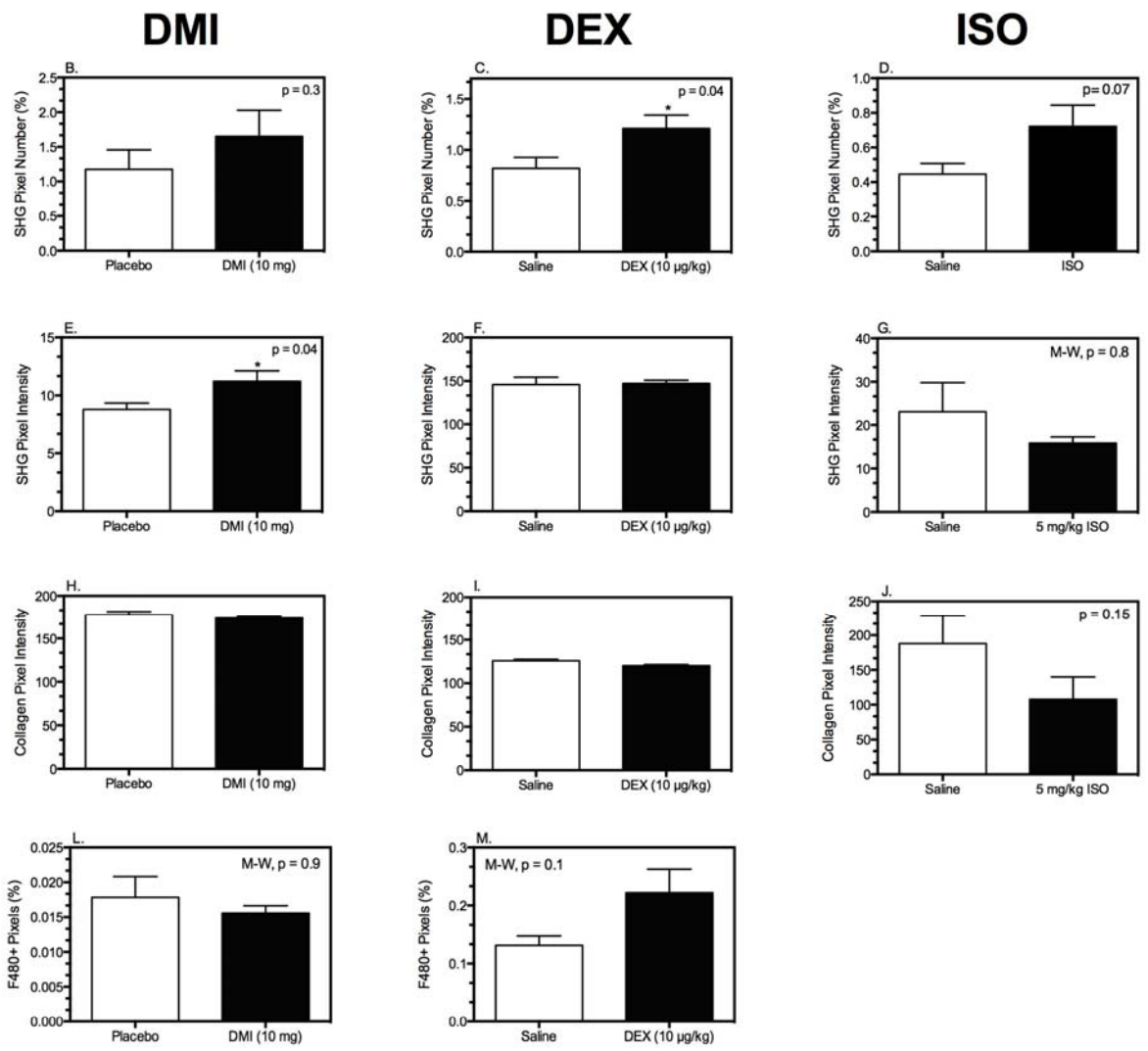

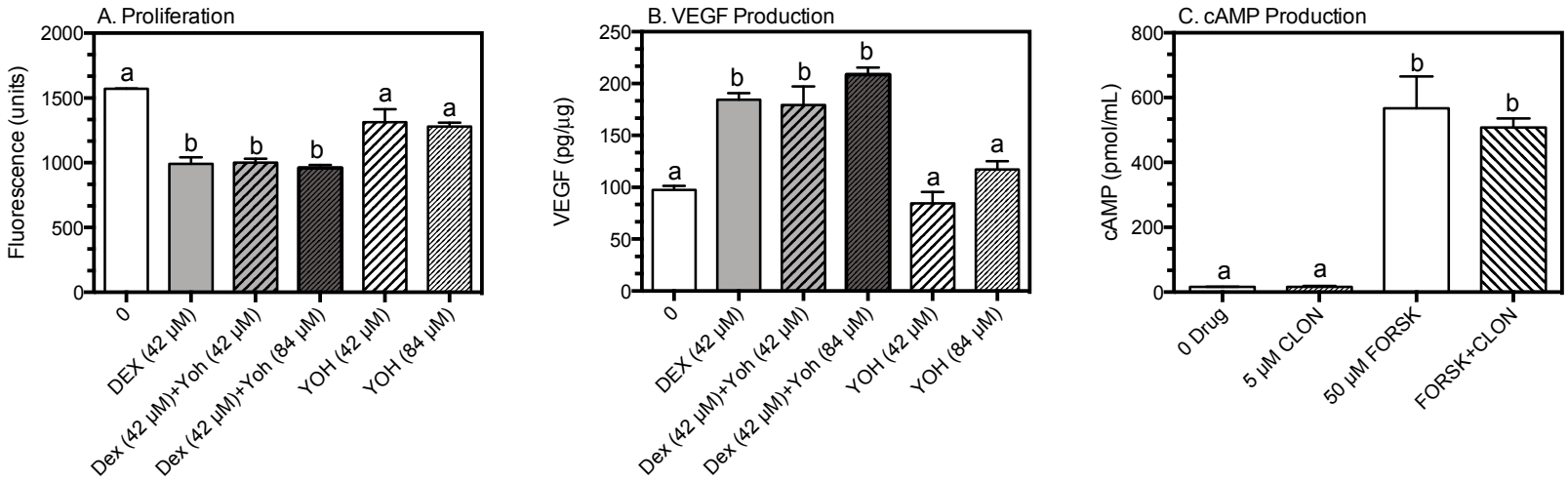

Supplemental Fig. S1. 4T1 Cells Do Not Express Functional α_2-AR. High dose DEX-induced effects on 4T1 (A) proliferation and (B) VEGF production *in vitro* are not blocked by the α_2-AR antagonist yohimbine (YOH). (C) The alpha$_2$-AR agonist clonidine (CLON) did not inhibit forskolin (FORSK)-induced cAMP. Results expressed as mean ± SD of duplicate wells, representative of 2 experimental repetitions. (A-C) One-way ANOVA revealed significant main effects ($p<0.002$). Groups labeled 'a' are not significantly different from each other, but are significantly different from groups labeled 'b', $p\leq0.01$, Tukey's post-hoc test.

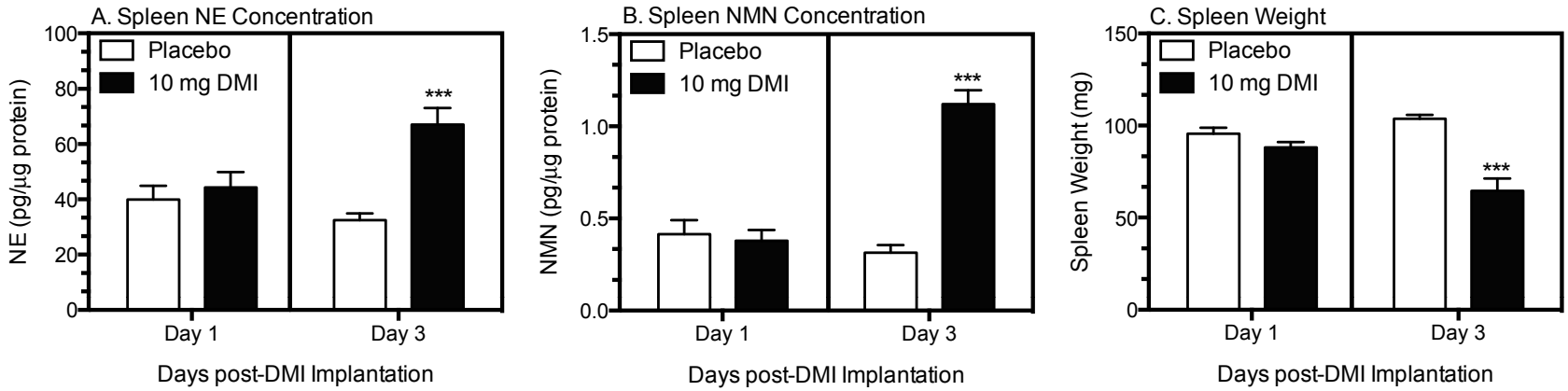

Supplemental Fig. S2. DMI Elevates Spleen Norepinephrine (NE) and the NE Metabolite, Normetanephrine (NMN). Spleen (A) NE and (B) NMN were increased 3 days post-DMI pellet implantation. (C) Spleen weight was decreased day 3 post-DMI implantation. Results expressed as mean ± SEM, n=6 per group. (A-C) Two-way ANOVA revealed significant main effects of DMI treatment ($p=0.0001$) and treatment by time interactions ($p\leq0.006$). *** indicates significant differences versus the corresponding placebo group, Holm-Sidak multiple comparison test, $p<0.001$.

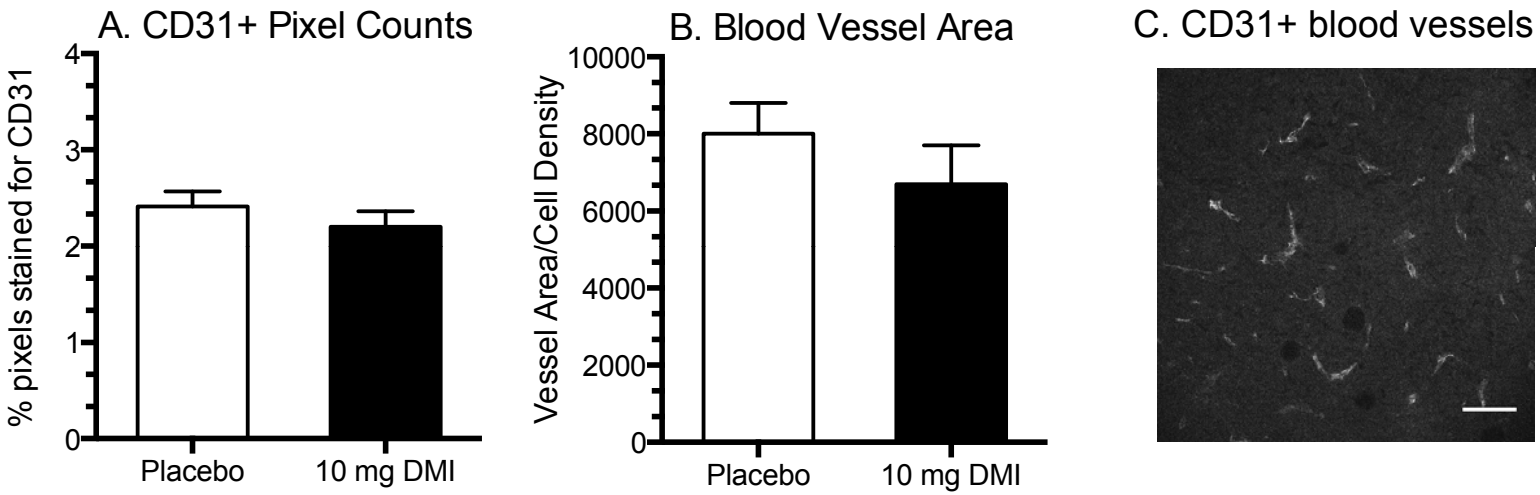

Supplemental Fig. S3. DMI-induced Tumor Growth is Not Associated with Altered Tumor Angiogenesis. Mice implanted with placebo (n=9) or 10 mg DMI (n=9) pellets were sacrificed 14 days after 4T1 inoculation. Immunocytochemical staining of CD31+ blood vessels in tumor slices were quantified by two different methods: (A) percentage of pixels above threshold in each image and (B) tracing vessels and calculating the area of the traced vessels per cell density. Cell density was determined by thresholding based on nuclear DAPI staining (not shown). (C) A representative image of CD31+ blood vessels. Scale bar = 50 μm. Results expressed as mean ± SEM. No significant differences were detected in either A or B.

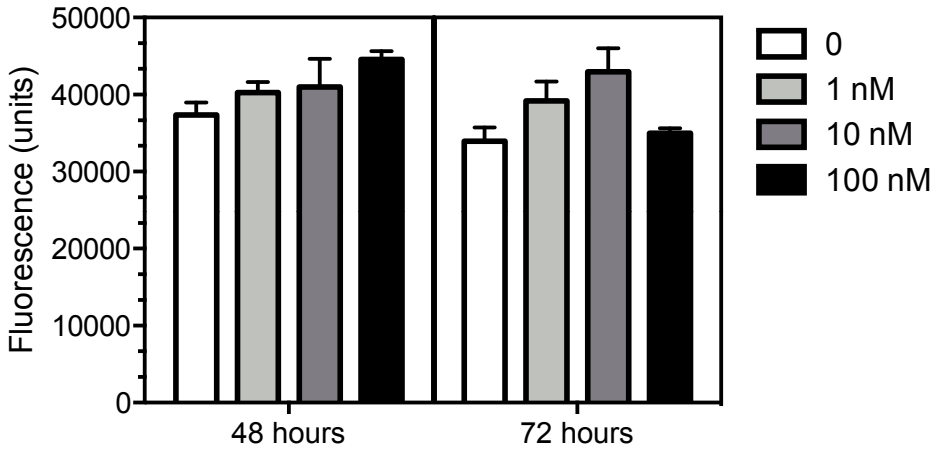

Supplemental Fig. S4. TNF-α Does Not Induce 4T1 Proliferation in Vitro. TNF-α was added at varying doses to 4T1 cells. Proliferation was measured 48 and 72 hours later. Results are expressed as mean ± SD of triplicate wells. Two-way ANOVA, no significant main effect of treatment ($p=0.12$) or interaction ($p=0.09$).